https://doi.org/10.5194/egusphere-2026-2576
Preprint. Discussion started: 11 May 2026

Consistency Between Zonal Mean Stratospheric and Total Column Ozone Trends (2000-2024)

Brian Auffarth[1], Mark Weber[1], Alexei Rozanov[1], Carlo Arosio[1], John P. Burrows[1], Melanie Coldewey-Egbers[2], Sean M. Davis[3], Doug Degenstein[4], Kimberlee Dubé[4], Stacey M. Frith[5,6], Lucien Froidevaux*[7], Diego Loyola[2], Vitali E. Fioletov[8], Viktoria Sofieva[9], Ronald van der A[10], and Jeannette D. Wild*[11, 12]

[1]Institute of Environmental Physics,University of Bremen, Bremen, Germany
[2]DLR (German Aerospace Center), Oberpfaffenhofen-Wessling, Germany
[3]NOAA Chemical Sciences Laboratory, Boulder, CO, USA
[4]University of Saskatchewan, Saskatoon, Canada
[5]Adnet Systems, Inc., Lanham, MD, USA
[6]NASA Goddard Space Flight Center, Greenbelt, MD, USA
[7]Jet Propulsion Laboratory, Pasadena, CA, USA
[8]Environment and Climate Change Canada, Toronto, Canada
[9]FMI (Finnish Meteorological Institute), Helsinki, Finland
[10]KNMI (Royal Netherlands Meteorological Institute), De Bilt, The Netherlands
[11]ESSIC/University of Maryland, College Park, MD, USA
[12]NOAA NESDIS/STAR, College Park, MD, USA
* Retired

Correspondence: Brian Auffarth (brian@iup.physik.uni-bremen.de)

Abstract.

This study presents an updated assessment of stratospheric and total column ozone trends over the 2000-2024 period using six merged limb-profile datasets and six merged total ozone datasets. Long-term changes were quantified using a multiple linear regression framework that accounts for dynamical and chemical variability. In addition to standard regressors (solar cycle, QBO, ENSO, stratospheric aerosol optical depth), we include Arctic and Antarctic Oscillation indices and the eddy heat flux in each hemisphere as proxies for dynamic variability. Volcanic (and wildfire) aerosol forcing is represented by separate proxies for three periods dominated by the major volcanic events of El Chichón, Pinatubo, and post-2000 volcanic eruptions, including Hunga-Tonga. These period-specific proxies are employed to better account for varying dynamical ozone responses that largely depend on the season and location of the eruptions. All profile datasets consistently show positive trends in the upper stratosphere, with the strongest ozone recovery in southern mid-latitudes, in agreement with other studies. In the lower stratosphere, trends remain weak, spatially heterogeneous, and predominantly negative. A comparison of stratospheric column trends derived from profile data with total ozone trends shows close agreement across latitude bands. Within the trend uncertainties, total column trends since 2000 are largely driven by stratospheric ozone changes, while tropospheric contributions to zonal-mean total ozone trends (the difference between total and stratospheric column trends) appear negligible. The extended regression framework improves the representation of recent dynamical variability and provides an updated perspective on stratospheric ozone recovery through 2024.

https://doi.org/10.5194/egusphere-2026-2576
Preprint. Discussion started: 11 May 2026

1 Introduction

The stratospheric ozone layer absorbs the sun's ultraviolet radiation, which is harmful to humans and the planet's environment (e.g. Bornman et al., 2023). With the depletion of global stratospheric ozone through the 1990s due to ozone-depleting substances (ODS) (Solomon, 1999), the ozone layer was significantly weakened, especially in the polar regions during spring, i.e. the ozone hole (Farman et al., 1985). The enactment of the Montreal Protocol in 1987 and its Amendments phased out ODS to counteract this decrease in ozone (Velders et al., 2007; WMO, 2018). A slow but gradual ozone recovery on the order of 1-2 %/decade above around 35 km in the upper stratosphere is evident (e.g. Steinbrecht et al., 2017; Sofieva et al., 2017; Ball et al., 2018; Petropavlovskikh et al., 2019; Szeląg et al., 2020; Li et al., 2023; Sofieva et al., 2023), coinciding with the decline of stratospheric halogens released from the ODS (Bernath and Fernando, 2018; Steffen et al., 2019; Froidevaux et al., 2022). The upper stratospheric trends remain robust and nearly unchanged after ozone timeseries updates to the end of 2024 (Sofieva et al., 2025).

In addition to ODS, atmospheric dynamics and changes in greenhouse gases also significantly influence ozone, particularly, in the lower stratosphere (Chipperfield et al., 2015; WMO, 2022). Ozone trends in the lower stratosphere are in some cases negative but have larger uncertainties and are often not statistically different from zero (Godin-Beekmann et al., 2022), although statistically significant trends have been reported in some studies. Ball et al. (2018, 2019) reported negative trends ranging from the tropics to mid-latitudes. Most chemistry-climate models predict ozone decreases in the tropical lower stratosphere ozone decreases and increases in the extratropics due to a strengthening of the Brewer-Dobson circulation in a changing climate (e.g. Ball et al., 2020), which is in contradiction to Ball et al. (2018, 2019) showing negative trends in the extratropics. Since total ozone trends show negligible trends in the tropics (Weber et al., 2022), it was hypothesised that increases in tropical tropospheric ozone may have balanced decreases in the lower stratosphere (Ball et al., 2018).

Because of the rather limited lifetime of individual satellite missions (up to a maximum of 20 years), merged ozone datasets are needed to analyse ozone trends over several decades. These datasets are the combination of multiple satellite measurements of ozone profiles merged into a single 40+ year coherent dataset. In this study, we use a multiple linear regression (MLR) and apply it to six long-term ozone profile datasets and six long-term total ozone datasets to analyze ozone variability and trends over the time period from 2000 to 2024.

In previous multiple linear regression (MLR) studies of total ozone trends additional dynamical proxies, like the Arctic and Antarctic Oscillation (AO/AAO) and hemispheric eddy heat fluxes representing the Brewer-Dobson circulation, were needed to properly model the large variability in extratropical total ozone (Chehade et al., 2014; Weber et al., 2022). These dynamical proxies were not used in the most comprehensive and recent ozone profile trend study by Godin-Beekmann et al. (2022) and Sofieva et al. (2025). Both studies use the so-called LOTUS model setup (Petropavlovskikh et al., 2019).

Applying the same MLR settings to both total column and vertical profile data shall allow us to answer the question of how much stratospheric and total column trends differ, providing some estimates of the tropospheric contributions (i.e. the differences between total and stratospheric column trends).

https://doi.org/10.5194/egusphere-2026-2576
Preprint. Discussion started: 11 May 2026

The major objective of this study is to assess post-2000 ozone trends through 2024 using multiple independent merged profile and total column datasets. While continued upper-stratospheric recovery has been recently confirmed (Sofieva et al., 2025), the magnitude and hemispheric structure of post-2000 trends, particularly in the lower stratosphere and polar regions, remain sensitive to methodological choice in the MLR setup, including proxy selection and treatment of volcanic forcing. Lower stratospheric (around 5 km above the tropopause) ozone has the largest contribution to total column ozone.

By comparing standard regression configurations like the LOTUS setup with an extended proxy setup that explicitly represents dynamical variability (AO, AAO, and eddy heat flux) and separates major volcanic aerosol periods, including the latest period that is dominated by the Hunga Tonga-Hunga Ha'apai (HTHH) volcanic event, we evaluate the relative contributions of stratospheric versus tropospheric changes to total column trends. Our approach allows us to distinguish chemically driven long-term recovery from dynamically induced variability and trends, acknowledging that chemistry–dynamics coupling may limit a strict separation..

This paper is structured as follows. Section 2 summarises briefly the details on the merged ozone datasets. Section 3 describes the conversion of some of the profile data to a common altitude grid (geometric altitude) and ozone units (number density). The unit conversions are necessary for calculating stratospheric columns from the ozone profiles. Uncertainties arising from the conversion are assessed. In addition, the long-term drifts between the datasets are investigated. Section 4 summarises the MLR setup and the proxy settings. Results are reported in Section 5, followed by a discussion (Section 6) and summary (Section 7).

2 Data

To ensure a consistent analysis of long-term ozone trends, this study uses a harmonized (common altitude and ozone unit) set of monthly mean datasets (Table 1). Both vertically resolved ozone profile data and total column ozone datasets are included to provide a comprehensive picture of ozone trends. Since the individual profile datasets differ in their vertical and latitudinal grids, as well as in ozone units, all ozone monthly mean profiles are converted to common grids and units before further analysis. Reanalysis data from ERA5 and reference measurements from Aura MLS are used to perform and evaluate these conversions, respectively, ensuring internal consistency across datasets.

Related publications to the merged datasets are listed in the Data Availability section at the end of the paper.

2.1 Ozone profile datasets

This study uses six long-term merged limb satellite ozone profile datasets: GOZCARDS (Global OZone Chemistry And Related trace gas Data records for the Stratosphere), SAGE-CCI-OMPS (SAGE II, Climate Change Initiative and OMPS), SAGE-OSIRIS-OMPS (SAGE II, OSIRIS and OMPS), SAGEII-OSIRIS-SAGEIII (SAGE II, OSIRIS and SAGE III), SAGE-SCIA-OMPS (SAGE II, SCIAMACHY and OMPS), and SWOOSH (The Stratospheric Water and Ozone Satellite Homogenized). All datasets provide monthly zonal mean stratospheric ozone profiles and are widely used for long-term trend analyses (e.g. Steinbrecht et al., 2017; Godin-Beekmann et al., 2022; Sofieva et al., 2023, 2025). Most datasets begin in 1984/1985 with the launch of SAGE-II, while GOZCARDS extends back to 1979, providing the longest record. All datasets are extended until

https://doi.org/10.5194/egusphere-2026-2576
Preprint. Discussion started: 11 May 2026

the end of 2024, enabling consistent post-2000 trend analyses. The temporal coverage of contributing instruments is shown in Figure 1, and dataset characteristics including latitude coverage, vertical range, ozone units, and contributing instruments are summarized in Table 1. The datasets employ different merging strategies, including anomaly-based merging, debiased absolute-value merging, and absolute-value merging with retained seasonal structure. Despite these methodological differences, all datasets are internally consistent, quality-controlled, and suitable for assessing long-term stratospheric ozone trends. For consistency, all ozone profile datasets are converted to a common latitude–altitude grid and unified ozone units (Sect. 3.1).

A more detailed description of the datasets is given by Steinbrecht et al. (2017) and Davis et al. (2026).

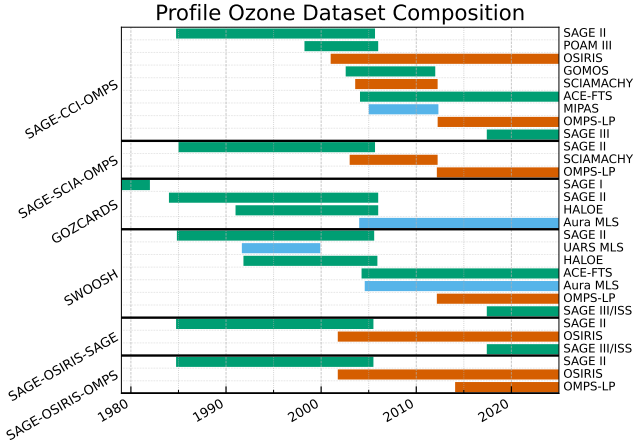

Figure 1. Satellite missions contributing to each of the six merged ozone profile datasets.

2.2 Total ozone datasets

Six long-term merged total column ozone datasets: MSR2 (Multi-sensor re-analysis), GSG (GOME/SCIAMACHY/GOME2), GTO-ECV (GOME-type Total Ozone - Essential Climate Variable), SBUV (Solar Backscatter Ultraviolet) NASA (MOD (Merged Ozone Data Set)), SBUV NOAA (COH (Cohesive)), and WOUDC (World Ozone and Ultraviolet Radiation Data Centre) are analysed. All datasets extend through the end of 2024 and provide quality-controlled estimates of total ozone suitable for long-term trend analysis. The zonal mean total ozone records generally begin earlier than the profile datasets, with start dates from 1960 (WOUDC) and 1970 (SBUV-MOD). SBUV-COH starts in 1978, while GTO-ECV and GSG start in 1995. In the MLR, the latter two datasets are extended back in time to 1978, the starting year of the regression, using the SBUV-COH data (Weber et al., 2022). The temporal coverage, latitudinal range, and contributing instruments of each dataset are summarized in Table 1, while the contribution of individual instruments is illustrated in Figure 2.

The datasets comprise a mix of satellite-only merged products and one dataset based upon ground-based observations (WOUDC). The MSR2 dataset provides globally gridded total ozone fields based on data assimilation using individual data records that are bias corrected using groundbased data from Brewer and Dobson instruments (van der A et al., 2015). The

https://doi.org/10.5194/egusphere-2026-2576
Preprint. Discussion started: 11 May 2026

remaining satellite products apply homogenization and bias-corrections to match individual data records. WOUDC complements the satellite records by providing independent zonal mean data derived from ground-based total ozone measurements from Dobson, Brewer, and filter instruments. Zonal mean ground data are calculated combining station data and an ozone climatology (Fioletov et al., 2002, 2008).

More details on the various merged datasets can be found in Weber et al. (2022) and Davis et al. (2026).

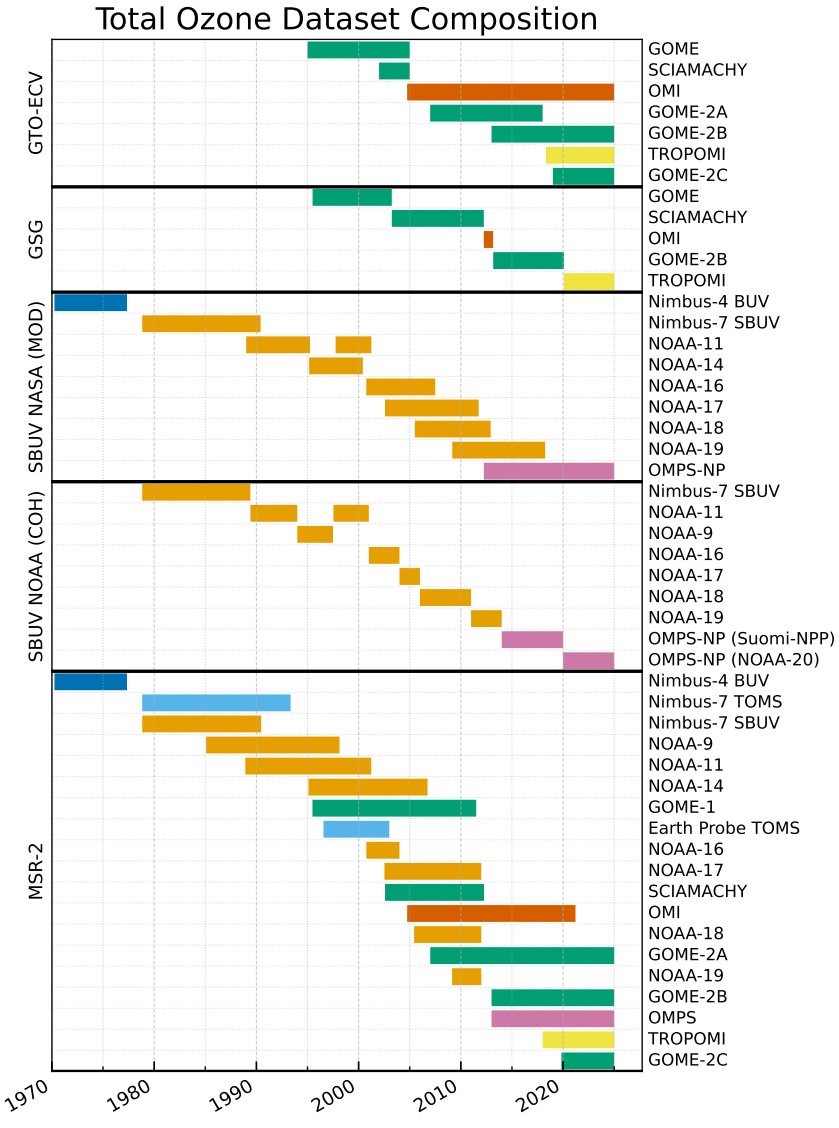

Figure 2. Same as Figure 1, but for the six merged total ozone datasets.

https://doi.org/10.5194/egusphere-2026-2576
Preprint. Discussion started: 11 May 2026

Table 1. Overview of merged ozone datasets used in this study, including their temporal coverage, spatial resolution, and original ozone units.

Dataset	Time period	Latitude	Vertical range	Ozone Unit	Instruments
Profile ozone datasets					
GOZCARDS v2.2	1979–2024	85° S to 85° N	215–0.1 hPa	mol/mol	SAGE I, SAGE II, HALOE, Aura MLS
SAGE-CCI-OMPS+	1984–2024	85° S to 85° N	10–50 km	molec/m^3	SAGE II, OSIRIS, GOMOS, MIPAS, SCIAMACHY, ACE-FTS, OMPS-LP (UBr, USask), SAGE III/ISS, POAM III
SAGE-OSIRIS-OMPS	1984–2024	60° S to 60° N	10–50 km	molec/cm^3	SAGE II, OMPS-LP (USask), OSIRIS
SAGE-SCIA-OMPS v4.1	1985–2024	85° S to 85° N	8-60 km	molec/cm^3	SAGE II, SCIAMACHY, OMPS-LP (UBr)
SAGEII-OSIRIS-SAGEIII	1984–2024	60° S to 60° N	10–50 km	molec/cm^3	SAGE II, SAGE III/ISS, OSIRIS
SWOOSH v2.71	1984–2024	85° S to 85° N	316–1 hPa	ppmv	SAGE II, SAGE III/ISS, UARS HALOE, UARS MLS, Aura MLS, ACE-FTS
Total ozone datasets					
MSR2	1970–2024	87.5° S to 87.5° N	Total column	DU	BUV-Nimbus4, TOMS-Nimbus7, TOMS-EP, SBUV-Nimbus7, NOAA 9/11/4/16/17/18/19, GOME, SCIAMACHY, OMI, GOME-2, OMPS, TROPOMI
GSG	1995–2024	87.5° S to 87.5° N	Total column	DU	GOME, SCIAMACHY, GOME-2B, OMI, TROPOMI
GTO-ECV	1995–2024	82.5° S to 82.5° N	Total column	DU	GOME, SCIAMACHY, OMI, GOME-2A/B/C, TROPOMI
NASA SBUV/OMPS (MOD) v8.7	1970–2024	77.5° S to 77.5° N	Total column	DU	Nimbus-4 BUV, Nimbus-7 SBUV, NOAA 11/14/16/17/18/19 SBUV/2, Suomi NPP OMPS
NOAA SBUV/OMPS (COH) v8.6	1978–2024	77.5° S to 77.5° N	Total column	DU	Nimbus-4 BUV, Nimbus-7 SBUV, NOAA 9/11/16/17/18/19 SBUV/2, Suomi NPP OMPS
WOUDC	1964–2024	87.5° S to 87.5° N	Total column	DU	Dobson, Brewer, and filter instruments

https://doi.org/10.5194/egusphere-2026-2576
Preprint. Discussion started: 11 May 2026

2.3 Auxilliary datasets used for assessing uncertainties in unit conversion

For this study we need all ozone profile datasets in units of number densities [molec cm^{-3}] as a function of geometrical altitude [km]. This conversion is needed to directly compare the ozone trends in absolute units and will help in calculating the stratospheric column. The conversion was applied to GOZCARDS and SWOOSH (see Table 3). Meteorological data (geopotential height, pressure, and temperature) from the ERA5 re-analysis data were used for the conversion of the datasets (Hersbach et al., 2020). Apart from the uncertainties in reanalysis temperatures, the conversion applied to monthly mean data, as provided in the merged data product, may lead to uncertainties compared to a merged data product based upon single ozone profiles converted before taking the monthly means. The conversion of individual ozone profiles before averaging, gridding, and merging is considered to be more accurate, but is not possible here. We quantify this additional uncertainty using Aura MLS (Microwave Limb Sounder) ozone and temperature observations.

MLS, aboard NASA's Aura satellite, provides high vertical resolution ozone profiles spanning from the upper troposphere into the mesosphere (Waters et al., 2006). The long-term stability of Aura MLS has been assessed in comparison to ground-based data (e.g. Hubert et al., 2016) and MLS is, therefore, suitable for assessing the conversion uncertainty.

3 Data Preparation

3.1 Ozone unit and vertical grid conversion

The limb ozone profile merged datasets (Table 1) are level 3 (L3) monthly mean zonal mean datasets having different ozone units, vertical grids, and spatial resolutions. For a direct comparison of the profile ozone trends, we convert the datasets to common ozone units and vertical grid and re-bin them to a common spatial grid. The advantage of using number density and geometric altitude is the calculation of partial ozone column amounts (e.g. stratospheric) by simple vertical integration of the ozone profile. The units and altitude grid conversion are only needed for SWOOSH and GOZCARDS.

The common latitude grid is defined by the lowest available resolution of the profile datasets, which ranges from 85° S to 85° N (center latitudes) in 10° steps. The merged ozone datasets were created from level-2 (L2) orbit data. The unit conversion of the monthly mean L3, as done in this work, instead of L2 data, may contribute to trend uncertainties. To evaluate the impact of this conversion, we compared two conversion approaches using the MLS/Aura L2 data (2004-2022). The first approach converts the MLS L2 individual profiles to the common ozone and altitude units and afterward creates the monthly mean L3 data. The second approach first determines the L3 data and then applies the unit conversion to the monthly mean L3 data using monthly mean zonal mean meteorological parameters: temperature, pressure, and altitude from ERA5. The linear trends of the difference timeseries between both approaches give an estimate of the trend uncertainty resulting from the unit conversion.

Figure 3 shows the trend of the difference timeseries between both approaches as a function of latitude and month for selected altitude levels. Most of the trends are not significant (hatched areas). At 25 km, a negative trend of around 1 % per decade between April and August in the northern hemisphere (NH) and between January and July in the southern hemisphere (SH) is noted. The significance of these trends gets smaller with altitude, showing the most significant trends at 25 km. Especially in

https://doi.org/10.5194/egusphere-2026-2576
Preprint. Discussion started: 11 May 2026

the SH, insignificant trends are observed at higher altitudes (40 km). In general, we conclude that the trend uncertainty due to unit and altitude grid conversions is small and insignificant, but in selected regions and months non-negligible.

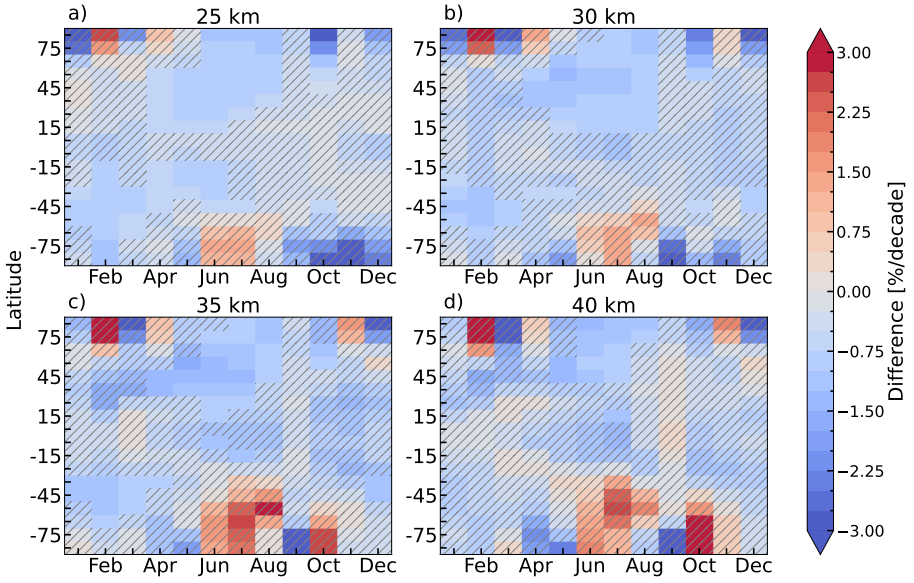

Figure 3. Zonal mean decadal trends of differences in %/decade from 2005 to 2022 between MLS L3 data converted after and before gridding at altitudes of 25, 30, 35 and 40 km (panels a to d). Hatches indicate insignificant trends within 2σ.

3.2 Relative Drifts among Multiple Datasets

Another contribution to uncertainties in long-term trends arises from relative drifts among the merged datasets. Here, relative drifts refer to systematic long-term differences between individual datasets and a common reference, in this case the multi-instrument mean (MIM). The spread of the drifts provides an estimate for possible contribution to trend uncertainties derived from multiple datasets.

To assess these relative drifts, a simple linear regression is applied to the time series of differences between the monthly mean merged datasets and the MIM. The drifts were calculated as follows. The percent ozone difference timeseries is calculated as follows for each profile dataset:

$$\Delta O_3(z,t) = 100 \cdot \frac{O_3(z,t) - \mathrm{MIM}(z,t)}{\mathrm{MIM}(z,t)}, \tag{1}$$

where O_3 is the ozone concentration of the merged dataset (in number density or DU). The linear trend (or relative drift) of the ΔO_3 timeseries from all datasets is computed, and the standard deviation of the mean of these trends represents the 1σ drift uncertainty, which is independent of the common reference, here MIM.

https://doi.org/10.5194/egusphere-2026-2576
Preprint. Discussion started: 11 May 2026

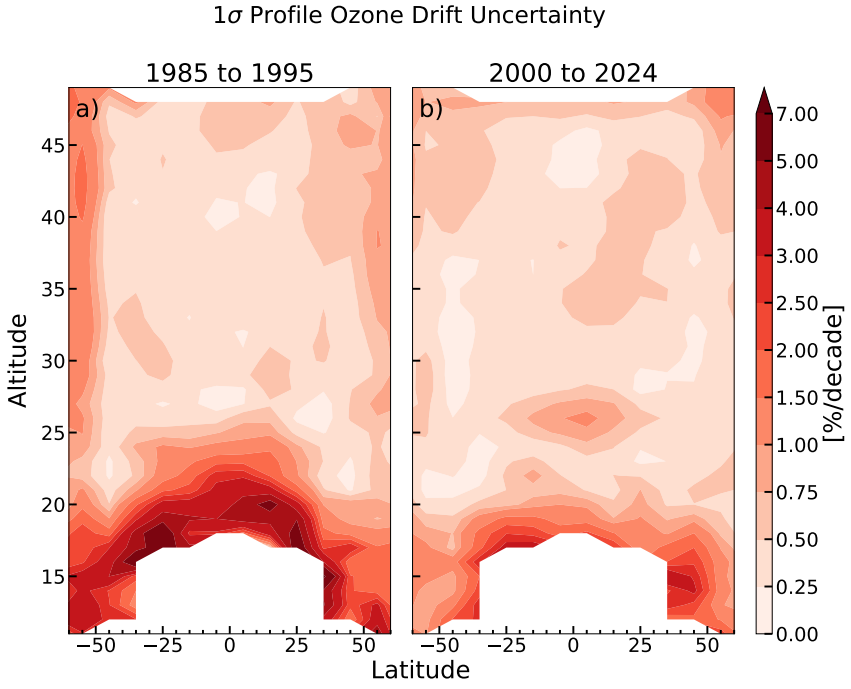

Figure 4. Standard deviation (1σ) of the drifts relative to the multi-instrument mean derived from GOZCARDS, SAGE-CCI-OMPS, SAGE-SCIA-OMPS, SAGE-OSIRIS-OMPS, SAGEII-OSIRIS-SAGEIII and SWOOSH profile data for the periods (a) 1985 to 1995 and (b) 2000 to 2024 as a function of latitude and altitude.

Figure 4 shows the 1σ drift uncertainty derived from the six merged profile datasets until 1995 and since 2000. It ranges from 0.5 to 0.75 %/decade between 60° S and 60° N and above 20 km. The uncertainties are larger at higher latitudes and lower altitudes and are most likely due to higher uncertainties in ozone measurements.

The same procedure was applied to the total ozone datasets, and results are shown for the period after 1996 (ODS peak) and 2000 in Figure 5. The drift uncertainty for the total ozone datasets is lower than for the profile datasets and range between 0.1 and 0.5 %/decade. The highest values can be seen at high latitudes and in the tropics, while the mid-latitudes show very low uncertainties.

4 Methods

4.1 Trend analyses

We apply a multiple linear regression (MLR) model to time series of ozone at each altitude-latitude grid point (for profile data) and each latitude (for total column data) including terms that account for various atmospheric processes, e.g. solar cyle, QBO, and El-Nino. The following equation shows the MLR equation (Godin-Beekmann et al., 2022; Sofieva et al., 2025) with

https://doi.org/10.5194/egusphere-2026-2576
Preprint. Discussion started: 11 May 2026

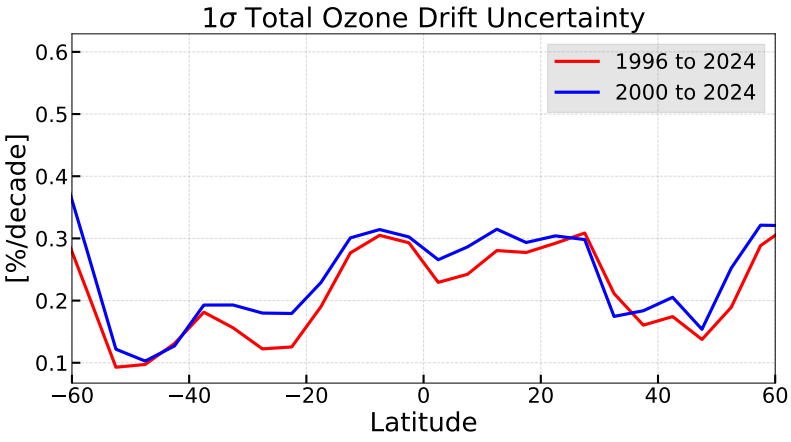

Figure 5. Standard deviation (1σ) of the mean of the drifts (1σ) derived from NASA SBUV, NOAA SBUV, GSG, GTO-ECV, and MSR2 total column data until 1995 and since 2000 as a function of latitude.

additional proxies as used in this study:

$$
\begin{aligned}
y(z,t) = {} & \beta_1(z,t)\cdot \mathrm{QBO}_1(t) + \beta_2(z,t)\cdot \mathrm{QBO}_2(t) + \beta_3(z,t)\cdot \mathrm{ENSO}(t) + \beta_4(z,t)\cdot \mathrm{Solar}(t) \\
& + \beta_5(z,t)\cdot \mathrm{SAOD}_{\mathrm{ElChichon}}(t) + \beta_6(z,t)\cdot \mathrm{SAOD}_{\mathrm{Pinatubo}}(t) + \beta_7(z,t)\cdot \mathrm{SAOD}_{\mathrm{HTHH}}(t) \\
& + \beta_8(z,t)\cdot \mathrm{AO}(t) + \beta_9(z,t)\cdot \mathrm{AAO}(t) + \beta_{10}(z,t)\cdot \mathrm{EHFS}(t) + \beta_{11}(z,t)\cdot \mathrm{EHFN}(t) \\
& + (\beta_{12}(z,t) + \beta_{13}(z,t)(t-t_1))\cdot L_{\mathrm{pre}}(t) + \beta_{14}(z,t)\cdot L_{\mathrm{Gap}}(t) + (\beta_{15}(z,t) + \beta_{16}(z,t)(t-t_2))\cdot L_{\mathrm{post}}(t) \\
& + \varepsilon(z,t)
\end{aligned}
\tag{2}
$$

with $y(z,t)$ being the monthly mean ozone as a function of altitude z and running month t and β_k the regression coefficients.

Terms containing L_{pre}, $L_{\mathrm{Gap}}(t)$, and L_{post} cover only consecutive periods with separate linear trend coefficients, β_{13} and β_{16}, before and after the ODS peak in 1996, respectively. These three variables are defined as follows:

$$
L_{\mathrm{pre}}(t) = \begin{cases} 1 & \text{if } t < t_0 \\ 0 & \text{if } t \geq t_0 \end{cases}, \tag{3}
$$

$$
L_{\mathrm{Gap}}(t) = \begin{cases} 0 & \text{if } t < t_0 \text{ and } t \geq t_1 \\ 1 & \text{if } t_0 \leq t < t_1 \end{cases}, \tag{4}
$$

and

$$
L_{\mathrm{post}}(t) = \begin{cases} 0 & \text{if } t < t_1 \\ 1 & \text{if } t \geq t_1 \end{cases}. \tag{5}
$$

https://doi.org/10.5194/egusphere-2026-2576
Preprint. Discussion started: 11 May 2026

t_0 is January 1996 and t_1, December 1999. Note that the term with $L_{\text{Gap}}(t)$ during the period 1996-1999 does not contain a linear trend fit coefficient. The main reason for this additional period is the sparse sampling of the merged ozone profile datasets. The global sampling of ozone profiles improves with more satellite instruments available after 2000 (Steinbrecht et al., 2017). Inclusion of the gap period allows for improved fitting of the proxy terms. Such a limitation is not given for the total ozone datasets.

To consider seasonality more explicitly, the regression model fits use harmonic terms to represent the annual and semi-annual cycles of selected terms, as shown in Eq. 6.

$$\beta_k(z,t) = \beta_{k0}(z) + \sum_{i=1}^{2}\left[\beta_{k1i}(z)\sin\left(\frac{2\pi it}{12}\right) + \beta_{k2i}(z)\cos\left(\frac{2\pi it}{12}\right)\right]. \tag{6}$$

Harmonic terms are only used for the QBO, ENSO, and fit coefficients in the trend terms (β_{12} to β_{16}). This approach is robust for non-deseasonalized data and helps reduce uncertainty in the estimated trend, particularly in datasets with sparse temporal coverage.

Trend uncertainties are derived from the covariance matrix of the regression coefficients. Since ordinary least squares assumes uncorrelated residuals, it tends to underestimate uncertainties when applied to ozone time series. To account for autocorrelation, we correct for first-order autocorrelation (AR-1) in the regression residuals (Cochrane and Orcutt, 1949). This is achieved by calculating the lag-1 autocorrelation and applying a transformation to the regression model that reduces the serial correlation of the residuals (Reinsel et al., 2002). The transformed regression equation provides the adjusted fitting coefficients and their uncertainties.

When reporting mean trends from multiple datasets, we use two different formulas for the uncertainty, explained in the LOTUS report and in more detail in Petropavlovskikh et al. (2019). For consistency with the previous analyses (Weber et al., 2022; Godin-Beekmann et al., 2022), we present both uncertainty estimates in our paper. First we use the LOTUS uncertainty estimate (Petropavlovskikh et al., 2019; Sofieva et al., 2025), which is defined as the maximum uncertainty of two terms:

$$\sigma^2_{\text{mean}} = \max\left(\frac{1}{N^2}\sum_{i,j} C_{ij}\sigma_i\sigma_j, \frac{1}{n_{\text{eff}}}\sum\frac{(x_i-\bar{x})^2}{N-1}\right). \tag{7}$$

The first term represents the variance of the mean of correlated trend estimates, accounting for the individual regression uncertainties and the correlations of model-data residuals. The LOTUS report uses constant correlation coefficients C_{ij} for the pre-1997 period and for the post-2000 period. In this paper we use latitude- and altitude-dependent correlation coefficients, which do not change the results substantially (Petropavlovskikh et al., 2019).

The second term is based on the sample variance of the individual trend estimates; the effective number of independent datasets, n_{eff} is defined as follows:

$$n_{\text{eff}} = \frac{N^2}{\sum_{i,j=1}^{N} C_{ij}} \tag{8}$$

https://doi.org/10.5194/egusphere-2026-2576
Preprint. Discussion started: 11 May 2026

(Petropavlovskikh et al., 2019). A second approach, the J-distribution, is a more conservative estimate and characterizes the total ensemble variance of trend estimates (Ko et al., 2013; Harris et al., 2015; Petropavlovskikh et al., 2019), which is defined as follows:

$$\sigma^2_{\text{mean}} = \frac{1}{N}\sum \sigma_i^2 + \sum \frac{(x_i - \bar{x})^2}{N-1}. \tag{9}$$

The first term accounts for uncertainties in the trends of the individual datasets and the second term represents the contribution from taking the statistical mean of the individual trends. The joint distribution is considered a conservative estimate (Ko et al., 2013) and produces larger uncertainties than other methods (Steinbrecht et al., 2017; Petropavlovskikh et al., 2019). Both the LOTUS estimate (Eq. 7) and the J-distribution (Eq. 9) consist of two components: the first arises from uncertainties in the MLR fit, while the second characterizes the spread of trend estimates across datasets. However, the two approaches differ in the interpretation of these terms. The J-distribution assumes that the dominant contribution to the MLR uncertainty, estimated from fit residuals, reflects unresolved variability not captured by the trend model. As a consequence, trend estimates from different datasets are effectively treated as fully correlated with respect to this component, and averaging does not reduce this contribution. In the case of $C_{ij} = 1$, the first terms in Eqs. (7) and (9) become identical. In contrast, the LOTUS estimate accounts for partial correlations between trend uncertainties, with correlation coefficients derived from fit residuals and ranging between approximately 0.6 and 0.95 for the datasets considered here. The second term in the J-distribution represents the full ensemble variance, whereas the LOTUS estimate corresponds to the standard error of the mean for correlated values. Since $n_{\text{eff}} \approx 1.4$ for the considered datasets, this term is only slightly reduced in the LOTUS formulation compared to the J-distribution. The J-distribution combines both contributions additively, while the LOTUS estimate uses the maximum of the two terms. For consistency with previous analyses Weber et al. (2022); Godin-Beekmann et al. (2022), both the LOTUS and J-distribution uncertainty estimates are used in this study. A detailed comparison of the two approaches is provided in Petropavlovskikh et al. (2019).

4.2 Proxy Setup

A list of the proxies used here is given in Table 2. The proxy timeseries have been normalized to the range from -0.5 to 0.5, except for the stratospheric aerosol optical depth (SAOD) (0 to 1 range). They have not been detrended, which means the dynamics-related trends are captured by the proxies rather than the linear trend terms. This way the linear trends approximate the long-term ODS-related ozone change (Weber et al., 2018). In contrast to the common proxy setup of the LOTUS model (Petropavlovskikh et al., 2019; Godin-Beekmann et al., 2022; Dubé et al., 2023; Sofieva et al., 2025), we add the Arctic and Antarctic Oscillation (AO/AAO), the Brewer-Dobson Circulation (BDC) as expressed by the eddy heat fluxes (EHFN, EHFS), and three separate SAOD proxies (Weber et al., 2022). Both EHFN and EHFS are proxies derived from ERA5 reanalysis ín the respective hemisphere (45°-75°). The Brewer-Dobson circulation in boreal and austral winter has an ozone response in the tropics opposite to that in the extratropics (e.g. Weber et al., 2011). There is also SH ozone response to the Brewer-

https://doi.org/10.5194/egusphere-2026-2576
Preprint. Discussion started: 11 May 2026

Dobson circulation in the NH (Fioletov and Shepherd, 2003). For this reason, EHFN and EHFS are included in the MLR for all latitudes. Similar arguments apply to AO/AAO proxies.

We chose these additional and dynamical regressors to better capture dynamic variability in ozone, such as the high ozone in the NH in 2024 (Newman et al., 2024). The Arctic Oscillation (AO), Antarctic Oscillation (AAO), and Brewer–Dobson circulation (BDC) proxies are winter/spring accumulated and weighted by the monthly ozone-variability to account for their seasonally integrated influence on stratospheric ozone (Weber et al., 2011, 2022). AO, AAO, EHFS, and EHFN regulate the meridional ozone transport into high latitudes from autumn through spring and accumulates ozone over winter/spring at high latitudes. They also regulate stratospheric temperatures in the polar region and, therefore, control the size of the polar vortices and associated polar chemical ozone loss (Newman et al., 2001; Weber et al., 2011). The low/high bias in spring ozone persists into summer, even though ozone variability decreases from spring to summer. By accumulating these proxies over the dynamically active season and weighting them by the monthly ozone variability, the regression model better captures the integrated ozone response. Extreme values in the timeseries are better captured by the regression model with the additional proxies (Weber et al., 2018, 2022). Figure 6 shows the regression coefficients of the proxy terms obtained from the MLR fit to SWOOSH data. The latitude-altitude distribution of the regression coefficients is as expected: the dominant lower stratospheric influence from the HTHH volcanic eruption (HTHH proxy) reducing ozone in the SH (e.g. Wang et al., 2023; Evan et al., 2023) and higher absolute values of EHFS and EHFN increasing ozone at high middle latitudes, as well as the strong influence of AO in the NH.

Table 2. Overview of proxies used in this study. Data are collected at https://www.iup.uni-bremen.de/OREGANO/proxy/ (last access: 2026-03-03)

Proxy	Time period	Dataset	MLR usage	Source
Solar	1979–2024	Mg II index	single	Snow et al. (2014)
Quasi-Biennial Oscillation (QBO)	1979–2024	Principal components of ERA5	harmonic	Hersbach et al. (2020)
AEROSOL El Chichon	1979–1989	GLOSSAC	single	Kovilakam et al. (2020)
AEROSOL Pinatubo	1990–1999	GLOSSAC	single	Kovilakam et al. (2020)
AEROSOL Hunga-Tonga	2000–2024	GLOSSAC	single	Kovilakam et al. (2020)
ENSO	1979–2024	ENSO 3.4 Index	harmonic	NOAA (c)
Arctic Oscillation (AO)	1978–2024	Arctic Oscillation[1,2]	single	NOAA (b)
Antarctic Oscillation (AAO)	1978–2024	Antarctic Oscillation[1,2]	single	NOAA (a)
Brewer-Dobson Circulation (BDC)	1979–2024	Eddy Heat Flux[1,2]	single	Hersbach et al. (2020)

[1] spring/winter accumulated

[2] ozone-variability weighted

In this study, the aerosol proxy is separated into three distinct time periods corresponding to the El Chichón period (1979–1989), the Pinatubo period (1990–1999), and the post-2000 period (2000–2024), which includes a series of medium volcanic erup-

https://doi.org/10.5194/egusphere-2026-2576
Preprint. Discussion started: 11 May 2026

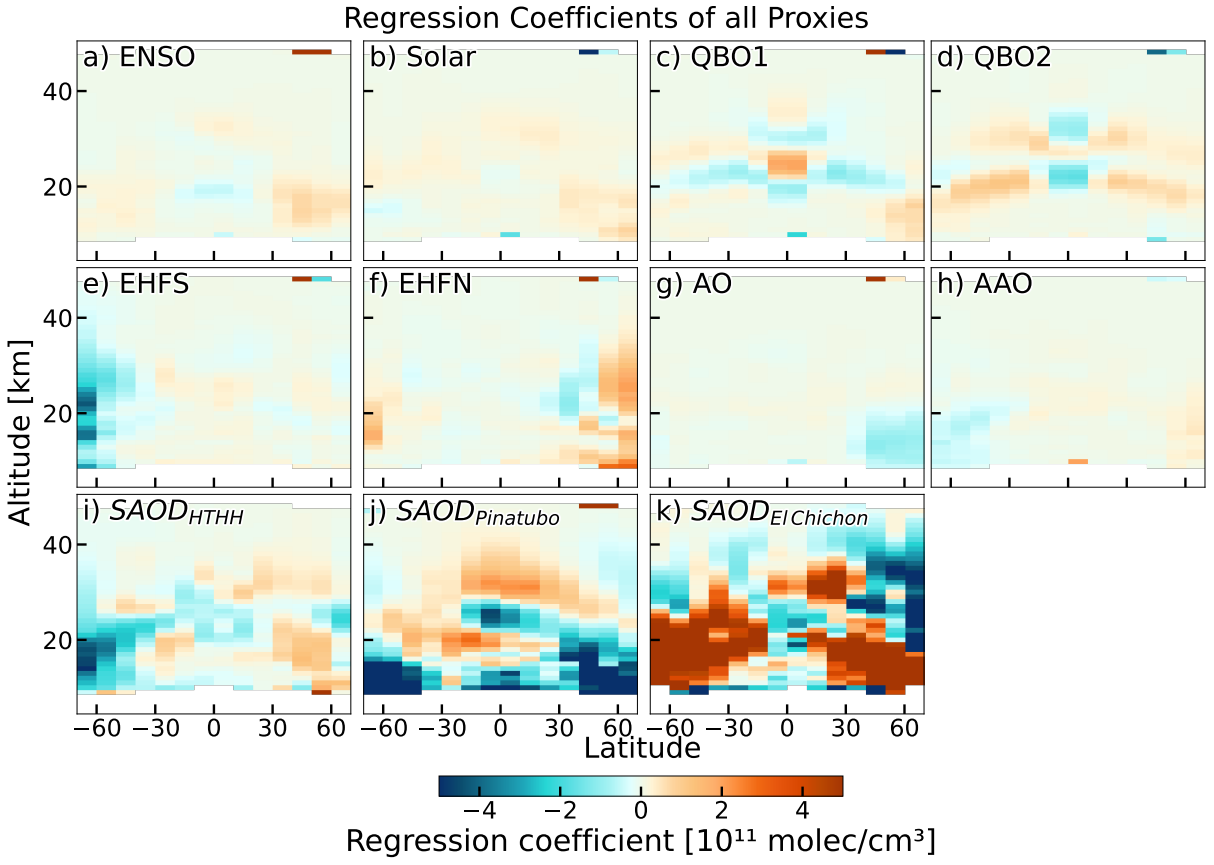

Figure 6. Regression coefficients for (a) ENSO, (b) Solar, (c) QBO1, (d) QBO2, (e) EHFS, (f) EHFN, (g) AO, (h) AAO, (i) SAOD (HTHH), (j) SAOD (Pinatubo) and (k) SAOD (El Chichon) from an MLR fit applied to SWOOSH. Note that EHFS proxy has the opposite sign of EHFN; therefore, lower (more negative) EHFS leads to increases in ozone.

tions as well as the HTHH eruption (Sofieva et al., 2024). Volcanic eruptions have markedly different impacts on stratospheric circulation, chemistry, and ozone distribution, depending on magnitude, season, and latitude of the event (Stolarski et al., 2006; Chehade et al., 2014). For this reason the major eruptions of El Chichón and Mount Pinatubo are treated separately in the regression. With the 2022 eruption of Hunga Tonga–Hunga Ha'apai (HTHH), a third strong volcanic event occurred that clearly affected stratospheric dynamics and composition (Zhu et al., 2025). Multiple SAOD proxies are also used because the eruptions of El Chichón and, in particular, Pinatubo produce substantially stronger and longer-lasting perturbations to ozone than later eruptions and thus dominate the regression if a single aerosol proxy is used. Treating these periods separately allows the regression model to better represent the variable volcanic forcing (Stolarski et al., 2006; Chehade et al., 2014).

The aerosol data are taken from the GLOSSAC climatologies (Kovilakam et al., 2020). The solar proxy is represented by the Mg II index time series (Snow et al., 2014). The Quasi-Biennial Oscillation (QBO) is described by the first two principal components from a PCA analysis of mean ERA5 stratospheric winds between -6° and 6° latitudes from 70 to 10 hPa. ENSO

https://doi.org/10.5194/egusphere-2026-2576
Preprint. Discussion started: 11 May 2026

is described by the ENSO 3,4 index time series. In the past, the El Niño–Southern Oscillation (ENSO) index (MEI V2, Wolter and Timlin (2011)) was used, but we suspect a possible drift starting in the early 2020s, making the index during the recent strong El Niño in 2023/24 too weak (Fig. A1. Additional seasonal components are added to the solar, QBO, and ENSO proxies as mentioned earlier.

5 Results

We applied the setup (Eq. 2) described in Sect. 4 to the six total ozone datasets and the six profile ozone datasets. Input to the MLR is the absolute timeseries of the datasets. While we mostly show trends from 2000 to 2024, the MLR is always applied to the longer period from 1979 (total ozone) and 1985 (ozone profiles) to 2024 with two inflection points starting in January 1996 and January 2000, with a gap period in between. In general, time series that we use for trend computation are filtered to ensure sufficient data coverage. We exclude time series with less than 50% valid observations for each sub-period defined by the inflection points. Additionally, we look for sufficient spread of data over each sub-period. For this, we want the first and last value of each period to span at least 50% of the entire time period, otherwise that period will be excluded from the analysis. This procedure effectively removes time series with insufficient data coverage, while also providing the highest amount of usable data for the trend analysis. The impact of these filters is mostly evident in the tropics below the tropopause and in high latitudes (above 60°) for the profile data and is small for total ozone column data.

5.1 Total Ozone Trends

We first evaluate the total ozone datasets (Table 1) for trends after 2000. The trends as a function of latitude (here in 5° steps), shown in Fig. 7, are mostly positive for all latitudes from 2000 to 2024. The blue lines show the results from our full setup, i.e., with dynamical proxies and three AOD, and the orange lines show the results for the so-called LOTUS setup, i.e., no dynamical proxies and single AOD. Most of the total ozone datasets agree very well. In the NH, total ozone recovers by $+1$ to $+1.5$ DU/decade ($+0.25$ to $+0.5$ %/decade). South of 40° trends increase on average to $+3$ to $+4$ DU/decade ($+1.3$ to $+1.5$ %/decade) using the full proxy setup. With the LOTUS settings, SH trends are lower and remain at about $+0.5$ DU/decade (see also Fig. A2 for the trends in %/decade). In the SH the difference between the two proxy setups is the strongest, while good agreement is seen elsewhere. The hemispheric asymmetry in the ozone trends with the full setup is in line with observations of the hydrogen chloride (HCl) asymmetry. Due to a faster circulation in the SH, HCl has declined faster, fostering in turn a faster increase in ozone compared to the NH (Chrysanthou et al., 2025; Dubé et al., 2025).

Results shown in Fig. 7 are very similar to results from Weber et al. (2022), who used a very similar proxy setup. The more positive SH trend that can be seen in their and our total ozone trends indicates the impact of these additional dynamical proxies. In our study we added a third SAOD proxy covering the period since 2000, dominated by the HTHH volcanic event.

To assess differences between the LOTUS model and the full regression model as well as the impact from using the third HTHH SAOD proxy, we look at selected modelled and observed total ozone timeseries. The MLR was applied to the September 60°S-90°S (ozone hole season) and the 35°S-60°S annual mean of the six datasets shown in Fig. 8). A slightly different MLR

https://doi.org/10.5194/egusphere-2026-2576
Preprint. Discussion started: 11 May 2026

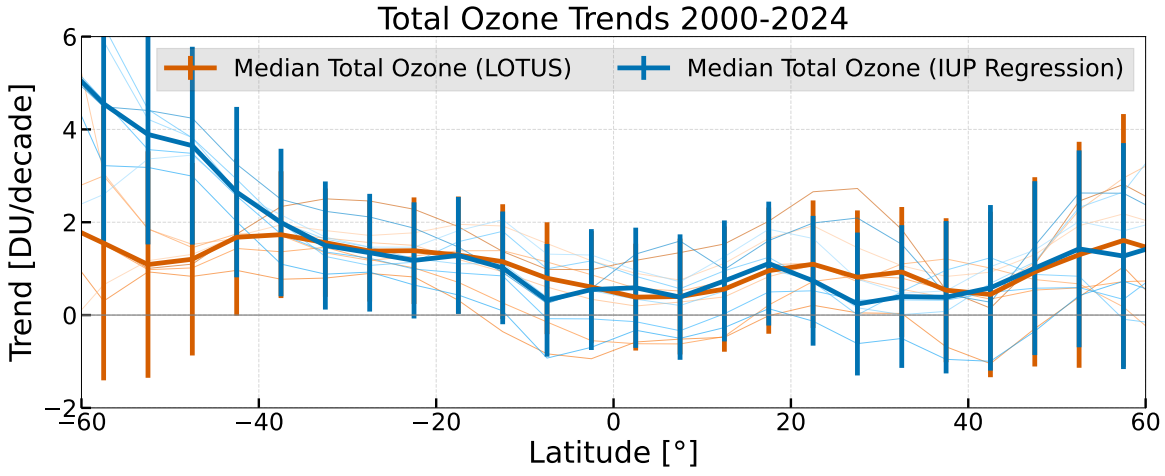

Figure 7. Total ozone trends in DU/decade from 2000 to 2024 for the six total ozone datasets WOUDC, SBUV NASA (MOD), SBUV NOAA (COH), GSG, GTO-ECV, and MSR2 (thin lines) and the median and its 2σ uncertainty (thick line and error bars). Shown in blue are the MLR results with additional dynamical and SAOD proxies and in orange the LOTUS model setup.

setup is used here, for a more direct comparison to previous analysis Weber et al. (2022): no gap terms, and in the polar region the pre-ODS period ends in 1999 and post-ODS peak period starts in 2000 (in the extrapolar region 1995 and 1996, respectively) (Newman et al., 2009; Weber et al., 2022). These results can be directly compared to results from Weber et al. (2022). For the southern mid-latitudes, Weber et al. (2022) report an annual trend of 0.7 %/decade for the period 1996–2020 applied to the median timeseries from five total ozone datasets. Extending the analysis to 2024, we obtain trends of 0.6 %/decade (panel c) and 0.4 %/decade with the LOTUS model (panel a). The inclusion of additional dynamical proxies improves the representation of short-term variability, particularly the local ozone minima in 2020-2022.

A higher difference between the MLR setup can be seen in the southern polar region, where ozone variability and chemical ozone depletion are strongly influenced by the dynamical processes. For September mean ozone between 60°S and 90°S, Weber et al. (2022) report a trend of 12.0 %/decade for 2000–2020. In contrast, we derive trends of 3.0 %/decade (LOTUS, panel b) and 8.2 %/decade (full regression), panel (d). Despite the low SH polar ozone in the early 2020s, the full regression trend, interpreted as the smooth ozone recovery related to ODS changes, remains stable within uncertainties after adding four additional years. The impact of dynamical proxies is most pronounced in the polar region (panel d). It is imperative to note, that the LOTUS setup (panel b) was not intended for use at polar latitudes and serves only as an illustration here. It is clear that specific polar proxies like polar stratospheric cloud (PSC) volume, are not needed to model polar ozone in winter/spring. Since there is a smooth transition in ozone response expected from middle to polar latitudes, the dynamical proxies are needed to reproduce consistent results (panel c and d).

https://doi.org/10.5194/egusphere-2026-2576
Preprint. Discussion started: 11 May 2026

To demonstrate the impact of the third SAOD ("HTHH") proxy, we look at the September trends in the SH polar region using different SAOD setups (panel d to f). Polar ozone recovery was first identified in the early phase of the ozone hole (e.g. Solomon et al., 2016; Weber et al., 2018; Stone et al., 2018). The first setup (panel e) uses a single AOD proxy for the complete time period like in the LOTUS setup, the second (panel f) uses two SAOD proxies, one until 1989 ("El Chichon") and from 1990 to 2024 ("Pinatubo") (Chehade et al., 2014; Weber et al., 2022), and the last (panel d) uses three SAOD proxies by adding the period 2000-2024 ("HTHH") and limiting the second SAOD to 1990-1999. The difference between the first (e) and the second (f) setup is small, with trends after 2000 being around +3.5 %/decade in both cases. The addition of the third (d) SAOD ("HTHH") more than doubles the post-2000 trend to 8.2 %/decade, making it very similar to +12.0 %/decade until 2020 from Weber et al. (2022). These results show the strong sensitivity of the regression and its influence in the southern polar region. Volcanic eruptions lead to perturbations in ozone that usually last for a few years (Wang et al., 2023; Fleming et al., 2024). In the early 2020s, a series of high-stratospheric aerosol events (Australian wildfires in 2019/2020, the 2021 Le Soufrière, and 2022 HTHH volcanic eruption) was responsible for the above-average size ozone holes between 2020 and 2023 (Yook et al., 2022; Fleming et al., 2024). The HTHH-SAOD proxy allows a better separation of these perturbations from the slow (background) decreases in ODS responsible for ozone recovery. The effect from the SAOD-HTHH proxy is however negligible for extrapolar total ozone, but the MLR pattern of the regression coefficient of the HTHH proxy shown in panel (i) of Fig. 6 seems physically reasonable. In summary, the use of the dynamical and SAOD-HTHH proxies in the MLR as well as the comparisons with the earlier results for the period ending in 2020 prove that ozone recovery is ongoing despite the ozone perturbations in the early 2020s in response to the series of volcanic and wildfire events.

5.2 Ozone profile trends 2000-2024

Figure 9 shows ozone profile trends as a function of latitude and altitude for the period 2000 to 2024 using the same setup as for total ozone (Eq. 2). Generally, there is good agreement between the datasets. Above 30 km the trends are below +0.1 DU/km/decade as ozone concentration decreases with altitude. Below 30 km, the ozone trends increase up to 0.5 DU/km/decade and contribute substantially to the total ozone trends. Negative trends with high uncertainties are mostly visible below 20 km, close to the tropopause. In the UTLS region, uncertainties in limb ozone measurements are higher and likely responsible for higher trend uncertainties (Rahpoe et al., 2015; Hubert et al., 2016).

Ozone profile trends in units of %/decade are shown in Fig. A3 of the Supplement. The trends observed in our study mostly agree with the results from (Sofieva et al., 2025), but there are some differences. The positive trends in the upper stratosphere are consistent between both studies (about +1 to +3 %/decade). A belt of negative trends just above the troposphere appears to be more persistent from 60°S to 60°N in Fig. 1 of Sofieva et al. (2025) and negative trends in the UTLS appear to be less negative in our case. This is also seen when comparing to a MLR setup without the AO, AAO, EHFS, and EHFN and with a single SAOD proxy (LOTUS setup), as shown in Figs. A4 and A5.

In the lower to middle stratosphere (above 20 km altitude), a hemispheric asymmetry in trends is noticeable, with higher trends in the SH, a pattern similar to what is observed for total ozone in Fig. 7. This asymmetry is also seen when looking at trends in three broad latitude bands. Figure 10 shows the ozone profile trends for the zonal bands, 35° S-60° S (SH), 20° S-

https://doi.org/10.5194/egusphere-2026-2576
Preprint. Discussion started: 11 May 2026

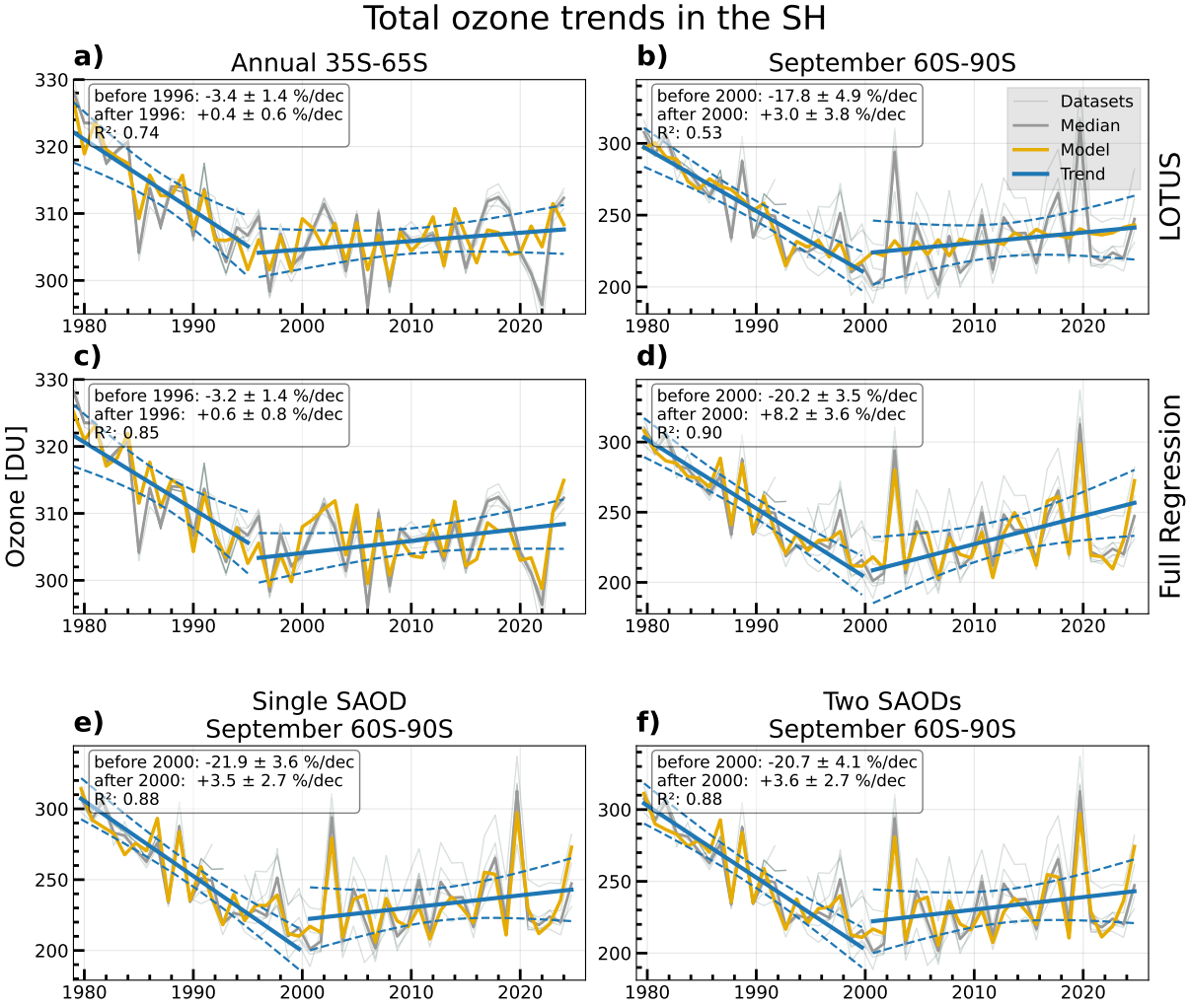

Figure 8. 35° S-60° S annual mean (panels a, c) and 60° S-90° S September (panels b, d, e, f) MLR results using the LOTUS setup (top row) and the full regression model (second row) applied the total ozone median from six merged datasets. Different SAOD setups are shown: (e) single AOD proxy from 1979 to 2024, (f) two AOD proxies: from 1979 to 1989 and from 1990 to 2024 and (d) three AOD proxies: from 1979 to 1989 (El Chichon period), from 1990 to 1999 (Pinatubo period), and from 2000 to 2024 (HTHH and smaller eruption period) are shown for the September SH polar region. Thick grey line: median of observations; yellow line: MLR regression; thin green lines: individual merged datasets; solid blue lines: trend lines before and after 2000; dashed blue lines: 2σ uncertainty of the trend lines.

https://doi.org/10.5194/egusphere-2026-2576
Preprint. Discussion started: 11 May 2026

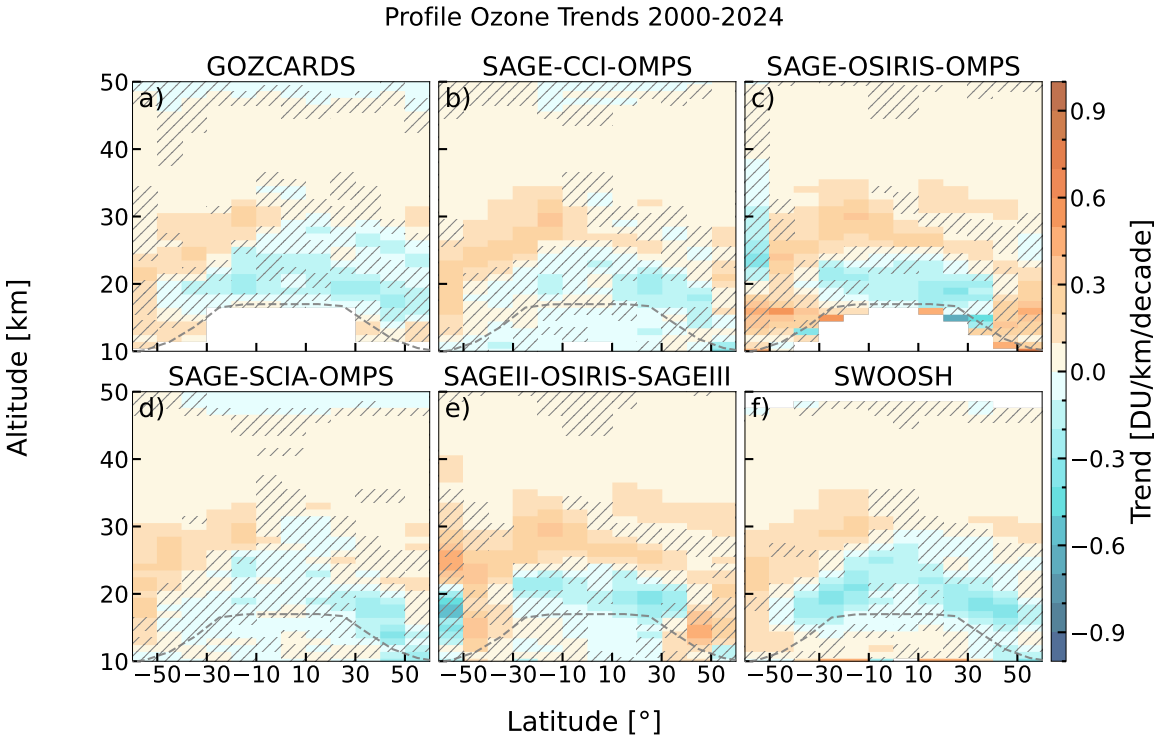

Figure 9. Profile ozone trends in DU/km/decade from 2000 to 2024 from the six merged ozone datasets as a function of latitude and altitude: (a) GOZCARDS , (b) SAGE-CCI-OMPS, (c) SAGE-OSIRIS-OMPS, (d) SAGE-SCIA-OMPS, (e) SAGEII-OSIRIS-SAGEIII, and (f) SWOOSH. Hatched areas indicate regions of no significance (2σ). Dashed lines are the climatological thermal tropopause derived from ERA5.

20° N (tropics) and 35° N-60° N (NH). Below 30 km altitude, trends are smaller in the NH compared to the SH. There is overall good agreement in the broad band trends between the datasets. All datasets agree on a positive trend above 30 km in all three latitude bands, maximizing at between 1-3 %/decade near 43 km altitude (Fig. A7). The SH displays larger variations in trends between datasets in this altitude region. The tropics show negative trends below 25 km for all datasets. In the extratropics trends below 20 km can be both positive and negative depending on the dataset. Below about 20 km altitude, the uncertainty in the mean trend increases.

The broad zonal band trends (Fig. 10) show the band trends, similar to Sofieva et al. (2025). The corresponding representation in % per decade Fig. A7) can can be compared with those shown in Fig. 4 of Sofieva et al. (2025), which were derived using the LOTUS setup and cover the same time period up to 2024. Upper stratospheric trends agree well between both studies. Differences are visible in the lower stratosphere. As mentioned before, the lowermost stratospheric mean trends are negative in the extratropics in Sofieva et al. (2025), while in our study they are positive in the SH and on average closer to zero in the NH (see also Figs. A8 and A9).

https://doi.org/10.5194/egusphere-2026-2576
Preprint. Discussion started: 11 May 2026

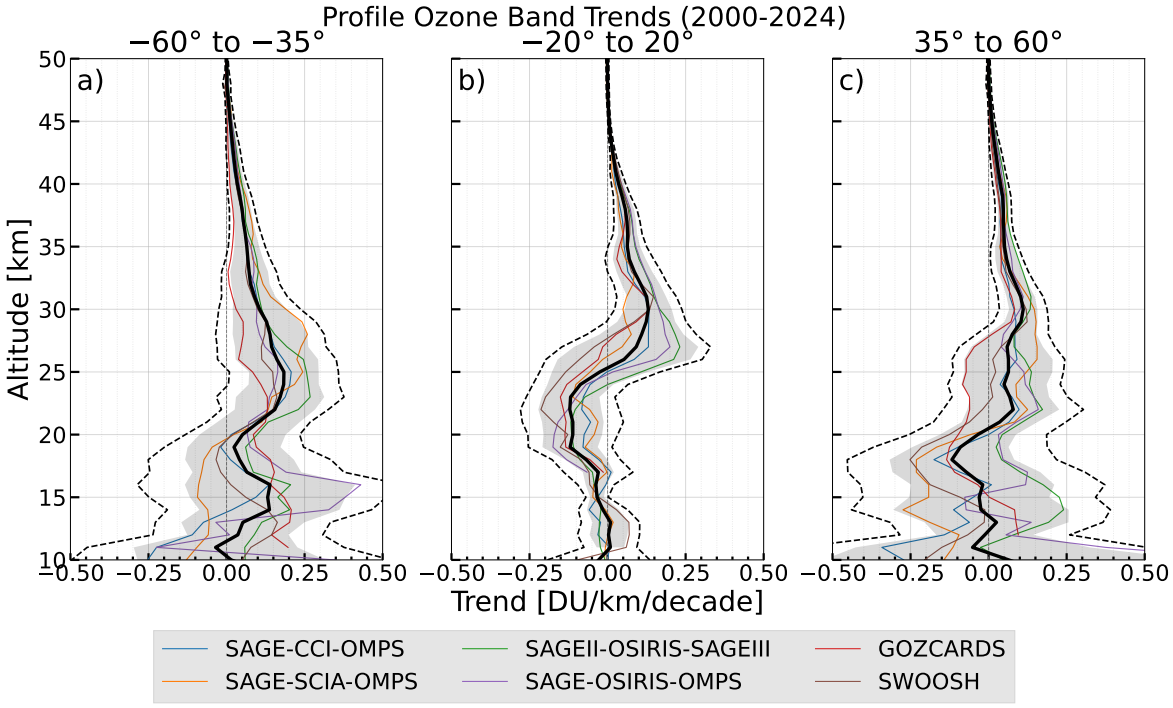

Figure 10. Ozone trends from 2000 to 2024 in three distinct broad latitude bands ((a)35° S-60° S, (b) 20° S-20° N, (c) 35° N-60° N) in DU/km/decade for the six merged ozone profile datasets: GOZCARDS, SAGE-CCI-OMPS, SAGE-OSIRIS-OMPS, SAGEII-OSIRIS-SAGEIII, SAGE-SCIA-OMPS, and SWOOSH. Shaded area indicates the 2σ uncertainties, calculated using the LOTUS uncertainty estimate described in Eq. 7 and the dashed line indicates the J-Distribution uncertainty described in Eq. 9 of the mean trends (black line).

The larger variations in SH trend profiles, seen in panel a) of Fig. 10 (see also Figs. A7-A9) is due to the smaller positive trends seen in GOZCARDS compared to all other merged datasets. Applying the MLR to deseasonalized ozone data (rather than absolute values), GOZCARDS trends in the SH are getting closer to the trends of the other data, as shown in Sofieva et al. (2025).

The differences between the LOTUS uncertainty estimate (shaded area) and the joint-distribution approach (dashed lines) are largest at lower altitudes, where the trends from the individual datasets show higher differences. This is particularly evident in the mid-latitudes around 17 km, most likely driven by both higher trend differences and differences in the underlying dataset uncertainties. While the LOTUS uncertainty estimate generally envelops the individual trends, with some exceptions for datasets exhibiting pronounced trends at specific altitudes, the joint-distribution approach spans a wider range, as it characterizes the total ensemble variance.

https://doi.org/10.5194/egusphere-2026-2576
Preprint. Discussion started: 11 May 2026

5.3 Comparison of total and stratospheric ozone column trends

We calculate the stratospheric columns by integrating the ozone profile upward from the ERA5 climatological thermal (lapse rate) tropopause. Another method to calculate the stratospheric ozone column trends is to integrate the ozone layer trends shown for example in Fig. 9. A comparison between the two methods (Fig. A6) show that the trends from both methods are generally very similar, however, the uncertainty of the vertically integrated layer trends are smaller than for the trend derived from stratospheric column trends. The tropopause height is determined at the center of each latitude band using interpolation. The MLR is then applied to the stratospheric columns. The difference between total column and stratospheric column trends can then be attributed to the tropospheric contribution to total ozone trends.

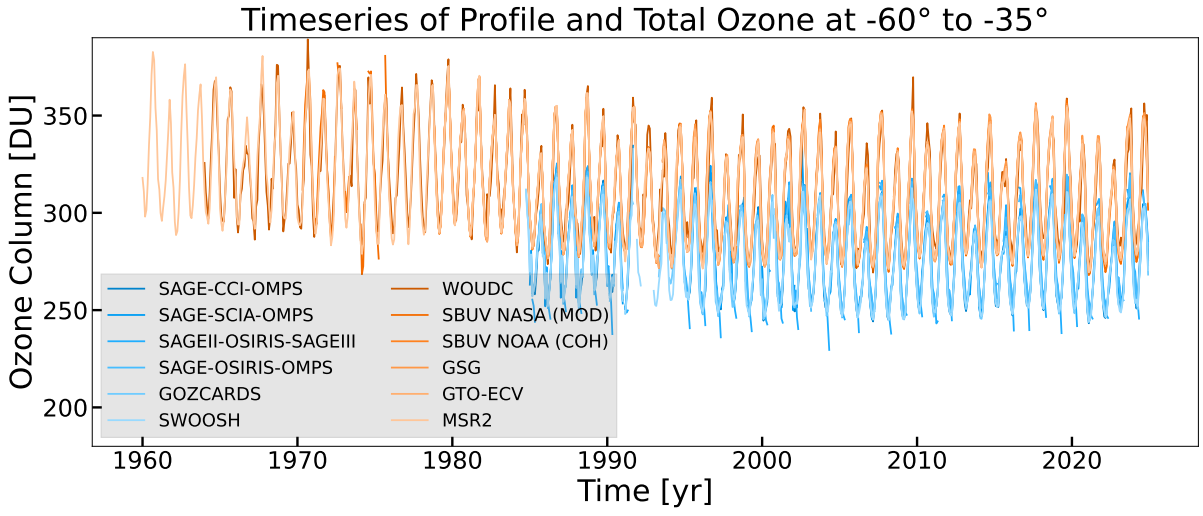

Figure 11. Observed zonal debiased mean stratospheric (blue) and total (orange) ozone columns in the 35° S to 60° S latitude band.

Figure 11 shows as an example the ozone timeseries in the broad zonal band 35° S-60° S for bias-corrected stratospheric ozone and total ozone columns of all datasets. The difference between the total and stratospheric columns of about 20 to 30 DU yields the zonal mean tropospheric column. There is a gap in the stratospheric column timeseries after the eruption of the Pinatubo volcano in 1992, because of filtering of columns that did not reach the tropopause. This is mainly due to retrieval artifacts in the presence of layers of high aerosols obstructing the limb view in the lowermost stratosphere. The total ozone datasets seem less affected. Due to the weaker eruption of HTHH in 2022 in terms of stratospheric aerosol load, this impact on stratospheric column calculation is also reduced except for SAGE-SCIA-OMPS. For this dataset, observations from February 2022 to May 2023 were excluded.

Figure 12 shows the results of the stratospheric column trends as a function of latitude which can be compared to the total ozone trends (Fig. 7). The tropics and the NH show very similar results with low ozone trends in the tropics (+0.0 to +1 DU/decade) and slightly higher ozone trends above 40°N (up to 2 DU/decade) for both proxy setups. The differences which we could see in the total ozone can be seen here as well in the SH. Trends using the full setup are larger (up to +3.5 DU/decade)

https://doi.org/10.5194/egusphere-2026-2576
Preprint. Discussion started: 11 May 2026

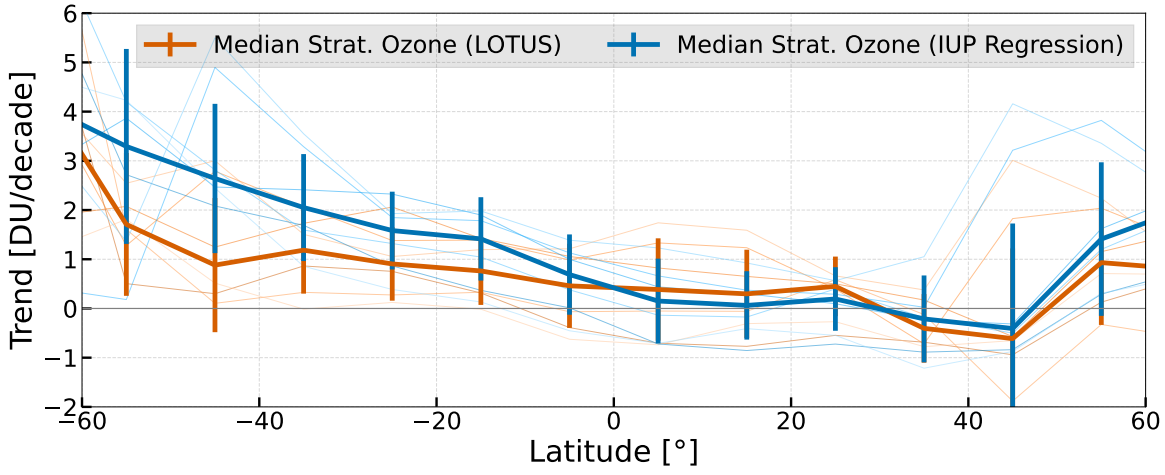

Figure 12. Stratospheric ozone trends in DU/decade from 2000 to 2024 for the six profile ozone datasets GOZCARDS, SAGE-CCI-OMPS, SAGE-OSIRIS-OMPS, SAGE-SCIA-OMPS, SAGEII-OSIRIS-SAGEIII and SWOOSH (thin lines) and the mean and its 2σ uncertainty (thick line and error bars). Shown in blue are the MLR results with additional dynamical and SAOD proxies and in orange the LOTUS model setup.

than using the LOTUS setup (+2 DU/decade). Both proxy setups yield similar trends in the SH for stratospheric and total columns, but the stratospheric column trends show a much higher spread between the trends of the different datasets compared to total ozone.

In Fig. 3b of Sofieva et al. (2025) combined latitude-dependent stratospheric column trends are shown and can be compared to our results. Above 40° latitude in each hemisphere stratospheric column trends using the LOTUS setup are slightly higher (around 2 DU/decade) in our analyses compared to Sofieva et al. (2025) (around 1 DU/decade). This difference likely arises from the comparatively strong trends in the OSIRIS dataset, which exert a larger influence on the multi-dataset mean in our six-dataset ensemble than in the eight-dataset mean used by Sofieva et al. (2025). Below 40° the stratospheric column trends agree.

Figure 13 shows trends for all datasets from 2000 to 2024 in the three broad zonal bands. The bars represent the stratospheric ozone column (light blue) and total ozone column trends (orange) of the individual merged datasets. The last two bars show the mean stratospheric ozone column (dark blue) and the mean total ozone column (brown).

The agreement between stratospheric and total column trends is remarkably close across all latitude bands (panels a to c). This suggests that the contribution of tropospheric ozone to the total column trends is small and well below the trend uncertainties of the total column trend. Significant positive stratospheric and total column trends are visible in the SH (about +2 to +4 DU/decade). On average, smaller trends (about +1 DU/decade) are seen in the tropics and the NH in agreement with Figs. 7 and 12. The two merged ozone profile datasets that include OSIRIS (SAGEII-OSIRIS-OMPS and SAGEII-OSIRIS-SAGEIII) show larger trends in comparison to the other ozone profile datasets in the extratropics. Both profile datasets that

https://doi.org/10.5194/egusphere-2026-2576
Preprint. Discussion started: 11 May 2026

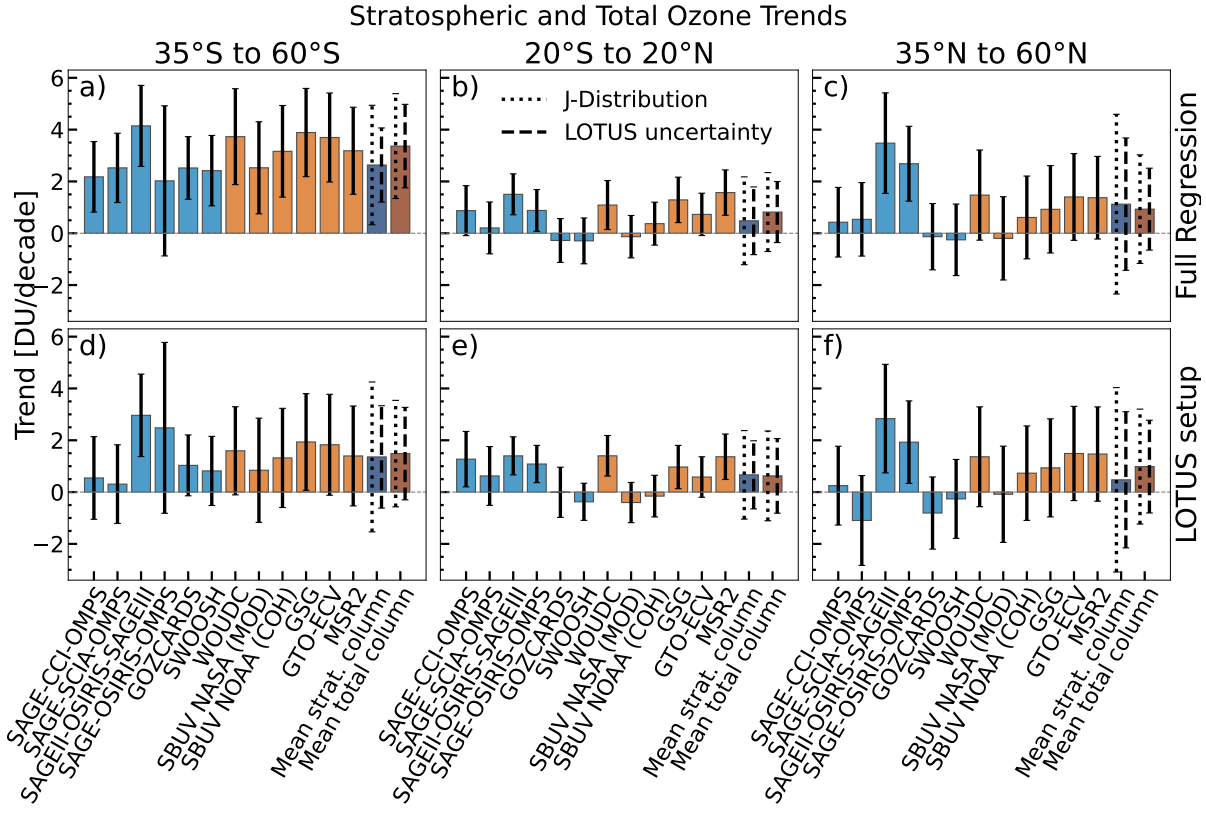

Figure 13. Broad band zonal mean ozone column trends from 2000 to 2024. Shown are total column trends (orange) and stratospheric column trends (blue) for each merged datasets. Upper row panels show the results using the full MLR regression and lower row panels show the regression with the LOTUS setup. Zonal bands are (a,d) 35° S to 60° S, (b,e) 20° S to 20° N, (c,f) 35° N to 60° N. Black error bars indicate the 2σ trend uncertainties. The last two bars in each panel show the mean stratospheric and total column ozone trends with two error bars each calculated using the LOTUS (dashed) and the J-distribution (dotted), respectively.

contain Aura/MLS at the end of their data record (GOZCARDS and SWOOSH) show, not unexpectedly, nearly the same trends.

The bottom row of Fig. 13 (panels d to f) shows our MLR results using the LOTUS setup. The mean profile trends are about +1 DU/decade in the SH and are smaller than with the full proxy setup except for the two merged datasets including OSIRIS and are mostly positive in the other two bands, similar to the full proxy trends.

The LOTUS and the J-distribution uncertainty estimates are showing similar results for total ozone, while the J-distribution uncertainty is mostly larger than the LOTUS uncertainty for the mean stratospheric column trends (Steinbrecht et al., 2017; Petropavlovskikh et al., 2019).

https://doi.org/10.5194/egusphere-2026-2576
Preprint. Discussion started: 11 May 2026

6 Discussion

The ozone profile datasets generally start at an altitude of 10 km (Table 1) which can be an issue when the tropopause is lower than 10 km, particularly at higher latitudes. For the stratospheric column calculations, data were screened out if more than three of the five layers above the tropopause had missing data. In combination with the larger uncertainties of limb measurements below 20 km, this selection criterion causes larger spreads in the profile and stratospheric column trends.

The conversion of the merged ozone profile datasets to a common vertical grid and ozone unit was done for GOZCARDS and SWOOSH and this leads to additional trend uncertainties as that conversion had to be applied to monthly mean data rather than single ozone profiles before merging. In most cases it was found that the difference between both conversions (monthly mean versus single profiles) is statistically not significant, but for certain altitude regions and months is non-negligible (Fig. 3). As these differences were mostly negative, the trends reported for GOZCARDS and SWOOSH may be slightly underestimated. To have a comparison of ozone trends on the same grid and with the same units as the other datasets, a conversion of pressure to geometric altitude and volume mixing ratio to number density was needed. The same method that was used for the other datasets to calculate the stratospheric column was then used for GOZCARDS and SWOOSH as well.

An additional uncertainty arises from temperature trends in the stratosphere. Conversion between pressure and altitude coordinates follows from the hydrostatic equation and therefore depends on atmospheric temperature. Long-term temperature changes induce vertical shifts of geometric altitude relative to pressure levels, which can alter vertical ozone gradients and modify the trends. As discussed by McLinden and Fioletov (2011) and in the LOTUS assessment (Petropavlovskikh et al., 2019), ozone trends derived on pressure levels (e.g., VMR) can differ from trends derived on altitude levels (e.g., number density) when substantial temperature trends are present. Before the late 1990s, pronounced upper-stratospheric cooling contributed to such discrepancies. For the post-2000 period analyzed in this paper, upper-stratospheric temperature trends are considerably weaker (e.g. Thompson et al., 2011). In the upper troposphere–lower stratosphere (UTLS), recent satellite-based analyses reveal vertically structured temperature trends and changes in lapse-rate tropopause height during the 21st century (Ladstädter et al., 2023; Ladstädter et al., 2025). Such structural changes may slightly affect local ozone gradients. However, given the comparatively small magnitude of recent temperature trends, temperature-driven effects are expected to remain a smaller contribution to the ozone trend estimates presented here.

A major point of discussion in this study concerns the choice of the proxy setup used in the MLR model. In contrast to the standard proxy configurations used in recent ozone trend studies (e.g., Godin-Beekmann et al. (2022); Sofieva et al. (2025)), we extended the set of independent variables to include the AO, AAO, and the BDC. We also separated the SAOD proxy into three distinct periods that included the large eruptions of El Chichon (1979-1999), Pinatubo (1990-1999), and Hunga-Tonga (2000-2024). Depending on the location and season of the eruptions, the dynamical response (circulation) from these eruptions may differ (e.g. Chehade et al., 2014). This expanded proxy configuration was chosen to better capture the dynamical and chemical variability observed in the past two decades (Weber et al., 2022). As shown in Fig. 8, the full regression is generalised in such a way that it covers the variability in and outside the polar region. The use of three SAOD proxies/periods brings total ozone trends at SH middle latitudes and the south polar region in better agreement with results from Weber et al. (2022), which

https://doi.org/10.5194/egusphere-2026-2576
Preprint. Discussion started: 11 May 2026

clearly indicate that the path of recovery remains within uncertainties unchanged from the earlier study, by using additional four years and despite lower ozone in the early 2020s. The HTHH-SAOD proxy to some extent likely also accounts for the effect from the enhanced water vapor following the underwater eruption of HTHH (Vömel et al., 2022; Millán et al., 2022). Changes in transport/circulation had a larger influence on ozone than altered chemistry due to enhanced chlorine activation following the eruption (Oesterstroem and Santee, 2025).

In total, the MLR model (Table: 2) includes 23 proxy variables together with the intercept and trend terms. While the number of fit parameters is higher than in most previous studies (Godin-Beekmann et al., 2022; Sofieva et al., 2025), the large temporal extent of the dataset, covering 24 years at a monthly resolution (288 data points per time series), provides sufficient degrees of freedom and does not necessarily imply overfitting, even in the presence of autocorrelation in the timeseries. We find that the inclusion of the AO, AAO, and BDC proxies improves the representation of inter-annual and sub-decadal variability, particularly during years with strong polar vortex disturbances. The change from a single AOD proxy to three independent AOD proxies (Figure 8) also improved the model by better capturing the seasonal ozone maxima and minima. While stratospheric and total column trends are very similar without and with the additional dynamical proxies (Figs. 7 and 12), the largest impact from the additional proxies is evident at middle to high latitudes in the SH, where LOTUS total ozone trends (+2 DU/decade) are half the values found in this study (+4 DU/decade). This indicates the impact of dynamics on ozone trends. The stratospheric column shows somewhat smaller differences between the two methods. The reason for this might come from the high variability of the ozone profile trends at high latitudes.

The histogram shown in Fig. 13 provides a very similar picture. Using the joint distribution (Ko et al., 2013) for calculating uncertainties, the 2σ uncertainties for the mean stratospheric and total column trends are mostly larger than the trends itself, except for the mean total ozone trends in the latitude band 35°S-60°S using the full proxy setup (panel a). Some contributions to the trend uncertainties are coming from the relative drifts between the datasets. After 2000 the 1σ-spread of drifts between ozone profile datasets is globally around 1 %/decade (+1 DU/decade) and increases strongly below 20 km (Fig. 4). For total ozone the 1σ-spread of drifts is about 0.1 to 0.3 %/decade (0.3 to 1 DU/decade) and also significantly contributes to the trend uncertainties (Fig. 5). Within uncertainties, the mean zonal stratospheric column trends do not differ from total ozone and the tropospheric ozone trend contribution (from the difference between both) is therefore not relevant..

Overall, the extended proxy setup provides a more comprehensive and physically consistent description of the processes influencing stratospheric and total ozone variability globally, and in particular, in the polar region (see Fig. 8).

But, as was briefly commented in Sect. 5, the ozone profiles and, with that, the stratospheric ozone trends have mostly large uncertainties and are also not as uniform in their trends as for total ozone. Such increased uncertainties in vertically resolved ozone, particularly close to the UTLS region, have also been reported recently by Davis et al. (2026), where discrepancies among observational ozone profile datasets, particularly in the lowermost stratosphere, were found. These uncertainties propagate into the derived stratospheric column ozone and therefore need to be considered when interpreting the computed trends.

https://doi.org/10.5194/egusphere-2026-2576
Preprint. Discussion started: 11 May 2026

7 Conclusion

We analyzed long-term ozone trends from 2000 to 2024 using multiple merged satellite profile and total column datasets. After harmonizing profile data to a common altitude grid, stratospheric column trends were calculated and compared directly with independent total ozone trends. Trends were estimated using a multiple linear regression model that includes an extended set of dynamical proxies to better capture inter-annual variability and recent circulation anomalies. All profile datasets consistently indicate continued ozone recovery in the upper stratosphere, particularly in southern mid-latitudes. In contrast, lower stratospheric trends remain weak and regionally variable, with negative tendencies in parts of the tropics. When integrated to stratospheric columns, the resulting trends closely match those derived from total column datasets across all latitude bands. Within statistical uncertainties, this agreement suggests that total ozone recovery since 2000 is primarily driven by changes in the stratosphere. Tropospheric ozone trends do not produce a detectable large-scale signal in total column trends over this period. The extended regression configuration improves the representation of recent high-variability years and volcanic influences. The main conclusions are positive upper-stratospheric trends and close agreement between total and stratospheric column changes within the combined trend uncertainties. These results provide an updated assessment of ozone recovery through 2024 and reinforce evidence that the Montreal Protocol continues to yield measurable atmospheric benefits.

8 Acknowledgement

BA, CA, AR, MW, and VS acknowledge the support by the European Space Agency (ESA) under Contract No. 4000137112/22/I-AG “Ozone Recovery from Merged Observational Data and Model Analysis (OREGANO)”.

The SBUV/OMPS-COH dataset was developed with support by NOAA Grant NA24NESX432C0001 (Cooperative Institute for Satellite Earth System Studies - CISESS) at the University of Maryland/ESSIC.

We acknowledge the important contributions by Ray Wang, John Anderson, and Ryan Fuller regarding the GOZCARDS merged ozone dataset. Work at the Jet Propulsion Laboratory, California Institute of Technology, was performed under contract with the National Aeronautics and Space Administration (80NM0018D0004). [Copyright 2026. All rights reserved.]

The development of GTO-ECV is funded by German Aerospace Center (DLR) and the EU Copernicus Climate Change Service (C3S).

9 Data availability

10 Code availability

All trends done in this study were computed with the IUP Regression Model, available from https://github.com/IUPBAuf/IUP-Regression-Model.

https://doi.org/10.5194/egusphere-2026-2576
Preprint. Discussion started: 11 May 2026

Table 3. Sources of the ozone datasets that were used in this study.

Dataset	Link	Reference
Profile ozone datasets		
GOZCARDS	https://disc.gsfc.nasa.gov/datasets/GozMmlpO3_1/summary	Froidevaux et al. (2015)
SAGE-CCI-OMPS	https://climate.esa.int/en/projects/ozone/data/	Sofieva et al. (2017)
SAGE-OSIRIS-OMPS	https://research-groups.usask.ca/osiris/	Bourassa et al. (2014)
SAGE-SCIA-OMPS	https://www.iup.uni-bremen.de/DataRequest/	Arosio et al. (2019)
SAGEII-OSIRIS-SAGEIII	https://research-groups.usask.ca/osiris/data-products.php	Bognar et al. (2022)
SWOOSH	https://csl.noaa.gov/groups/csl8/swoosh/	Davis et al. (2016)
Total ozone datasets		
MSR2	https://www.temis.nl/protocols/O3global.html	van der A et al. (2015)
GSG	https://www.iup.uni-bremen.de/UVSAT/data/wfdoas/	Weber et al. (2022)
GTO-ECV	https://atmos.eoc.dlr.de/gto-ecv	Coldewey-Egbers et al. (2015, 2022)
NASA SBUV/OMPS (MOD)	https://acdb-ext.gsfc.nasa.gov/Data_services/merged/	Frith et al. (2014, 2017)
NOAA SBUV/OMPS (COH)	https://www.star.nesdis.noaa.gov/data/smcd1/ozone/SBUV_OMPS_COH/	Larry Flynn & J. D. Wild, Personal Communication
WOUDC	https://woudc.org/archive/Projects-Campaigns/ZonalMeans/	Fioletov et al. (2002, 2008)

Author contributions. BA performed most of the data analysis and wrote the manuscript. MW supervised the study, contributed to writing the paper and provided the GSG data set. AR supervised the study and contributed to writing the paper. CA provided the SAGE-SCIA-OMPS data set and contributed to the review of the manuscript and the scientific outcome. JPB contributed to the review of the manuscript and the scientific outcome. MCD and DL provided the GTO-ECV data set and contributed to the review of the manuscript and the scientific outcome. SMD provided the SWOOSH data set and contributed to the review of the manuscript and the scientific outcome. DD and KD provided the SAGE-OSIRIS-OMPS and the SAGEII-OSIRIS-SAGEIII data sets and contributed to the review of the manuscript and the scientific outcome. SMF provided the NASA SBUV/OMPS (MOD) data set and contributed to the review of the manuscript and the scientific outcome. LF provided the GOZCARDS data set and contributed to the review of the manuscript and the scientific outcome. VEF provided the WOUDC data set and contributed to the review of the manuscript and the scientific outcome. VS provided the SAGE-CCI-OMPS data set and contributed to the review of the manuscript and the scientific outcome. RvA provided the MSR2 data set and contributed to the review of the manuscript and the scientific outcome. JDW provided the NOAA SBUV/OMPS (COH) data set and contributed to the review of the manuscript and the scientific outcome.

https://doi.org/10.5194/egusphere-2026-2576
Preprint. Discussion started: 11 May 2026

Competing interests. The contact author has declared that none of the authors have any competing interests.

Acknowledgements. BA, AR, MW, and VS are grateful for the financial support from the European Space Agency (ESA) via the OREGANO Project (Ozone Recovery from Merged Observational Data and Model Analysis, Contract No. 4000137112/22/I-AG).

https://doi.org/10.5194/egusphere-2026-2576
Preprint. Discussion started: 11 May 2026

References

Arosio, C., Rozanov, A., Weigel, K., Stiller, G., von Clarmann, T., Damadeo, R., Zawodny, J., Laeng, A., Sofieva, V., Kyrölä, E., et al.: Merged SAGE II, SCIAMACHY, and OMPS ozone profile dataset and evaluation of ozone trends in the stratosphere, Atmospheric Measurement Techniques, 12, 2423–2444, https://doi.org/10.5194/amt-12-2423-2019, 2019.

Ball, W. T., Alsing, J., Mortlock, D. J., Staehelin, J., Haigh, J. D., Peter, T., Tummon, F., Stenke, A., Anderson, J., Bourassa, A., Davis, S. M., Degenstein, D., Frith, S., Froidevaux, L., Roth, C., Sofieva, V., Wang, R., Wild, J., Yu, P., Ziemke, J. R., and Rozanov, E.: Evidence for a continuous decline in lower stratospheric ozone offsetting ozone layer recovery, Atmospheric Chemistry and Physics, 18, 1379–1394, https://doi.org/10.5194/acp-18-1379-2018, 2018.

Ball, W. T., Alsing, J., Staehelin, J., et al.: Stratospheric ozone trends for 1985–2018: sensitivity to recent large variability, Atmospheric Chemistry and Physics, 19, 12 731–12 747, https://doi.org/10.5194/acp-19-12731-2019, 2019.

Ball, W. T., Chiodo, G., Abalos, M., Alsing, J., and Stenke, A.: Inconsistencies between Chemistry–Climate Models and Observed Lower Stratospheric Ozone Trends since 1998, Atmospheric Chemistry and Physics, 20, 9737–9752, https://doi.org/10.5194/acp-20-9737-2020, 2020.

Bernath, P. and Fernando, A. M.: Trends in Stratospheric HCl from the ACE Satellite Mission, Journal of Quantitative Spectroscopy and Radiative Transfer, 217, 126–129, https://doi.org/10.1016/j.jqsrt.2018.05.027, 2018.

Bognar, K., Tegtmeier, S., Bourassa, A., Roth, C., Warnock, T., Zawada, D., and Degenstein, D.: Stratospheric ozone trends for 1984–2021 in the SAGE II–OSIRIS–SAGE III/ISS composite dataset, Atmospheric Chemistry and Physics, 22, 9553–9569, https://doi.org/10.5194/acp-22-9553-2022, 2022.

Bornman, J. F., Barnes, P. W., and Pandey, K.: Environmental effects of stratospheric ozone depletion, UV radiation, and interactions with climate change: 2022 Quadrennial Assessment, Photochemical & Photobiological Sciences, 22, 935–936, 2023.

Bourassa, A. E., Degenstein, D. A., Randel, W. J., Zawodny, J. M., Kyrölä, E., McLinden, C. A., Sioris, C. E., and Roth, C. Z.: Trends in Stratospheric Ozone Derived from Merged SAGE II and Odin-OSIRIS Satellite Observations, Atmospheric Chemistry and Physics, 14, 6983–6994, https://doi.org/10.5194/acp-14-6983-2014, 2014.

Chehade, W., Weber, M., and Burrows, J. P.: Total ozone trends and variability during 1979–2012 from merged data sets of various satellites, Atmospheric Chemistry and Physics, 14, 7059–7074, https://doi.org/10.5194/acp-14-7059-2014, 2014.

Chipperfield, M. P., Dhomse, S. S., Feng, W., McKenzie, R. L., Velders, G. J. M., and Pyle, J. A.: Quantifying the ozone and ultraviolet benefits already achieved by the Montreal Protocol, Nature Communications, 6, 15 371, https://doi.org/https://doi.org/10.1038/ncomms8233, 2015.

Chrysanthou, A., Dube, K., Tegtmeier, S., and Chipperfield, M.: Hemispheric Asymmetry in Stratospheric Trends of HCl and Ozone: Impact of Chemical Feedback on Ozone Recovery, Journal of Geophysical Research: Atmospheres, 130, https://doi.org/10.1029/2024JD042161, 2025.

Cochrane, D. and Orcutt, G. H.: Application of Least Squares Regression to Relationships Containing Auto-Correlated Error Terms, Journal of the American Statistical Association, 44, 32–61, https://doi.org/10.1080/01621459.1949.10483290, 1949.

Coldewey-Egbers, M., Loyola, D., Koukouli, M. E., Balis, D., Zimmer, W., Kiemle, S., Spurr, R., and Zehner, C.: The GOME-type Total Ozone Essential Climate Variable (GTO-ECV) data record from the ESA Climate Change Initiative, Atmospheric Measurement Techniques, 8, 3923–3940, https://doi.org/10.5194/amt-8-3923-2015, 2015.

https://doi.org/10.5194/egusphere-2026-2576
Preprint. Discussion started: 11 May 2026

Coldewey-Egbers, M., Loyola, D. G., Lerot, C., and Van Roozendael, M.: Global, regional and seasonal analysis of total ozone trends derived from the 1995–2020 GTO-ECV climate data record, Atmos. Chem. Phys., 22, 6861–6878, https://doi.org/10.5194/acp-22-6861-2022, 2022.

Davis, S., Ball, W., Jia, Y., Chiodo, G., Alsing, J., Keeble, J., Akiyoshi, H., Arosio, C., Bednarz, E., Chrysanthou, A., Coldewey-Egbers, M., Damadeo, R., Dhomse, S., Diallo, M., Dietmuller, S., Eichinger, R., Frith, S., Hassler, B., Hegglin, M., Hubert, D., Jöckel, P., Josse, B., Kramarova, N., Loyola, D., Maillard Barras, E., Marchand, M., Morgenstern, O., Plummer, D., Portmann, R., Rosenlof, K., Rozanov, A., Sofieva, V., Staehelin, J., Sukhodolov, T., Tourpali, K., Van Der A, R., Wang, H. J. R., Wargan, K., Watanabe, S., Weber, M., Wild, J., Yamashita, Y., and Ziemke, J.: Uncertainties in Recent Tropical Stratospheric and Tropospheric Ozone Changes Restrict Our Understanding of Future Total Column Ozone Change, EGUsphere [Preprint], https://doi.org/10.5194/egusphere-2026-532, 2026.

Davis, S. M., Rosenlof, K. H., Hassler, B., Hurst, D. F., Thorne, P. W., Barnett, J. J., Deaver, L., Remsberg, E., Tummon, F., and Weber, M.: The Stratospheric Water and OzOne Satellite Homogenized (SWOOSH) database: a long-term database for climate studies, Earth System Science Data, 8, 461–490, https://doi.org/10.5194/essd-8-461-2016, 2016.

Dubé, K., Tegtmeier, S., Bourassa, A., Zawada, D., Degenstein, D., Sheese, P. E., Walker, K. A., and Randel, W.: N_2O as a regression proxy for dynamical variability in stratospheric trace gas trends, Atmospheric Chemistry and Physics, 23, 13 283–13 300, https://doi.org/10.5194/acp-23-13283-2023, 2023.

Dubé, K., Tegtmeier, S., Ploeger, F., and Walker, K. A.: Hemispheric Asymmetry in Recent Stratospheric Age of Air Changes, Atmospheric Chemistry and Physics, 25, 1433–1447, https://doi.org/10.5194/acp-25-1433-2025, 2025.

Evan, S., Brioude, J., Rosenlof, K. H., Gao, R.-S., Portmann, R. W., Zhu, Y., Volkamer, R., Lee, C. F., Metzger, J.-M., Lamy, K., Walter, P., Alvarez, S. L., Flynn, J. H., Asher, E., Todt, M., Davis, S. M., Thornberry, T., Vömel, H., Wienhold, F. G., Stauffer, R. M., Millán, L., Santee, M. L., Froidevaux, L., and Read, W. G.: Rapid ozone depletion after humidification of the stratosphere by the Hunga Tonga Eruption, Science, 382, eadg2551, https://doi.org/10.1126/science.adg2551, 2023.

Farman, J. C., Gardiner, B. G., and Shanklin, J. D.: Large losses of total ozone in Antarctica reveal seasonal ClO_x/NO_x interaction, Nature, 315, 207–210, https://doi.org/10.1038/315207a0, 1985.

Fioletov, V. E. and Shepherd, T. G.: Seasonal Persistence of Midlatitude Total Ozone Anomalies, Geophysical Research Letters, 30, 1417, https://doi.org/10.1029/2002GL016739, 2003.

Fioletov, V. E., Bodeker, G. E., Miller, A. J., McPeters, R. D., and Stolarski, R.: Global and Zonal Total Ozone Variations Estimated from Ground-Based and Satellite Measurements: 1964–2000, Journal of Geophysical Research, 107, 4647, https://doi.org/10.1029/2001JD001350, 2002.

Fioletov, V. E., Labow, G., Evans, R., Hare, E. W., Köhler, U., McElroy, C. T., Miyagawa, K., Redondas, A., Savastiouk, V., Shalamyansky, A. M., Staehelin, J., Vanicek, K., and Weber, M.: Performance of the Ground-Based Total Ozone Network Assessed Using Satellite Data, Journal of Geophysical Research, 113, D14 313, https://doi.org/10.1029/2008JD009809, 2008.

Fleming, E. L., Newman, P. A., Liang, Q., and Oman, L. D.: Stratospheric Temperature and Ozone Impacts of the Hunga Tonga-Hunga Ha'apai Water Vapor Injection, Journal of Geophysical Research: Atmospheres, 129, e2023JD039 298, https://doi.org/10.1029/2023JD039298, 2024.

Frith, S. M., Kramarova, N. A., Stolarski, R. S., McPeters, R. D., Bhartia, P. K., and Labow, G. J.: Recent Changes in Total Column Ozone Based on the SBUV Version 8.6 Merged Ozone Data Set, Journal of Geophysical Research: Atmospheres, 119, 9735–9751, https://doi.org/10.1002/2014JD021889, 2014.

https://doi.org/10.5194/egusphere-2026-2576
Preprint. Discussion started: 11 May 2026

Frith, S. M., Stolarski, R. S., Kramarova, N. A., and McPeters, R. D.: Estimating Uncertainties in the SBUV Version 8.6 Merged Profile Ozone Data Set, Atmospheric Chemistry and Physics, 17, 14 695–14 707, https://doi.org/10.5194/acp-17-14695-2017, 2017.

Froidevaux, L., Anderson, J., Wang, H. J., Fuller, R., Schwartz, M. J., Santee, M. L., Livesey, N. J., Pumphrey, H. C., Bernath, P. F., Russell, J. M., and McCormick, M. P.: Global OZone Chemistry And Related trace gas Data records for the Stratosphere (GOZCARDS): methodology and sample results with a focus on ozone, Atmospheric Chemistry and Physics, 15, 10 471–10 507, https://doi.org/10.5194/acp-15-10471-2015, 2015.

Froidevaux, L., Kinnison, D. E., Santee, M. L., Millán, L. F., Livesey, N. J., Read, W. G., Bardeen, C. G., Orlando, J. J., and Fuller, R. A.: Upper Stratospheric ClO and HOCl Trends (2005–2020): Aura Microwave Limb Sounder and Model Results, Atmospheric Chemistry and Physics, 22, 4779–4799, https://doi.org/10.5194/acp-22-4779-2022, 2022.

Godin-Beekmann, S., Azouz, N., Sofieva, V. F., Hubert, D., Petropavlovskikh, I., Effertz, P., Ancellet, G., Degenstein, D. A., Zawada, D., Froidevaux, L., et al.: Updated trends of the stratospheric ozone vertical distribution in the 60°S–60° N latitude range based on the LOTUS regression model, Atmospheric Chemistry and Physics, 22, 11 657–11 673, https://doi.org/10.5194/acp-22-11657-2022, 2022.

Harris, N. R. P., Hassler, B., Tummon, F., Bodeker, G. E., Hubert, D., Petropavlovskikh, I., Steinbrecht, W., Anderson, J., Bhartia, P. K., Boone, C. D., Bourassa, A., Degenstein, D., Froidevaux, L., Fuller, R., Funke, B., Jones, A., Kyrölä, E., Laine, M., Lambert, J.-C., van der A, R., Sofieva, V., Tamminen, J., Tegtmeier, S., Thompson, A. M., Wild, J., and Zawodny, J.: Past changes in the vertical distribution of ozone - Part 3: Analysis and interpretation of trends, Atmospheric Chemistry and Physics, 15, 9965–9982, https://doi.org/10.5194/acp-15-9965-2015, 2015.

Hersbach, H., Bell, B., Berrisford, P., Hirahara, S., Horányi, A., Muñoz-Sabater, J., Nicolas, J., Peubey, C., Radu, R., Schepers, D., Simmons, A., Soci, C., Abdalla, S., Abellan, X., Balsamo, G., Bechtold, P., Biavati, G., Bidlot, J.-R., Bonavita, M., De Chiara, G., Dahlgren, P., Dee, D., Diamantakis, M., Dragani, R., Flemming, J., Forbes, R., Fuentes, M., Geer, A. J., Haimberger, L., Healy, S., Hogan, R. J., Hólm, E., Janisková, M., Keeley, S., Laloyaux, P., Lopez, P., Lupu, C., Radnoti, G., Rosnay, P., Rozum, I., Vamborg, F., Villaume, S., and Thépaut, J.-N.: The ERA5 global reanalysis, Quarterly Journal of the Royal Meteorological Society, 146, 1999–2049, https://doi.org/10.1002/qj.3803, 2020.

Hubert, D., Lambert, J.-C., Verhoelst, T., Granville, J., Keppens, A., Baray, J.-L., Cortesi, U., Degenstein, D. A., Froidevaux, L., Godin-Beekmann, S., Hoppel, K. W., Kyrölä, E., Leblanc, T., Lichtenberg, G., McElroy, C. T., Murtagh, D., Nakane, H., Querel, R., Russell, J. M., Salvador, J., Smit, H. G. J., Stebel, K., Steinbrecht, W., Strawbridge, K. B., Stübi, R., Swart, D. P. J., Taha, G., Thompson, A. M., Urban, J., van Gijsel, J. A. E., von der Gathen, P., Walker, K. A., Wolfram, E., and Zawodny, J. M.: Ground-based assessment of the bias and long-term stability of fourteen limb and occultation ozone profile data records, Atmospheric Measurement Techniques, 9, 2497–2534, https://doi.org/10.5194/amt-9-2497-2016, 2016.

Ko, M., Newman, P., Reimann, S., and Strahan, S., eds.: Lifetimes of Stratospheric Ozone-Depleting Substances, Their Replacements, and Related Species, SPARC Report 9, WCRP-15/2013, Deutsches Zentrum für Luft- und Raumfahrt (DLR), https://aparc-climate.org/publications/sparc-report-no-6/, 2013.

Kovilakam, M., Thomason, L. W., Ernest, N., Rieger, L., Bourassa, A., and Millán, L.: The Global Space-based Stratospheric Aerosol Climatology (version 2.0): 1979–2018, Earth System Science Data, 12, 2607–2634, https://doi.org/10.5194/essd-12-2607-2020, 2020.

Ladstädter, F., Steiner, A. K., Krasauskas, L., Ao, C. O., and Ho, S.-P.: Resolving the 21st century temperature trends of the upper troposphere–lower stratosphere with satellite observations, Atmospheric Chemistry and Physics, 23, xxxx–xxxx, https://doi.org/https://doi.org/10.1038/s41598-023-28222-x, 2023.

https://doi.org/10.5194/egusphere-2026-2576
Preprint. Discussion started: 11 May 2026

Ladstädter, F., Stocker, M., Scher, S., and Steiner, A. K.: Observed changes in the temperature and height of the globally resolved lapserate tropopause, Atmospheric Chemistry and Physics, 25, 16 053–16 062, https://doi.org/10.5194/acp-25-16053-2025, 2025.

Li, Y., Dhomse, S. S., Chipperfield, M. P., et al.: Quantifying stratospheric ozone trends over 1984–2020: a comparison of ordinary and regularized multivariate regression models, Atmospheric Chemistry and Physics, 23, 13 029–13 047, https://doi.org/10.5194/acp-23-13029-2023, 2023.

McLinden, C. A. and Fioletov, V.: Quantifying stratospheric ozone trends: Complications due to stratospheric cooling, Geophysical Research Letters, 38, https://doi.org/https://doi.org/10.1029/2010GL046012, 2011.

Millán, L., Santee, M. L., Lambert, A., Livesey, N. J., Werner, F., Schwartz, M. J., Pumphrey, H. C., Manney, G. L., Wang, Y., Su, H., Wu, L., Read, W. G., and Froidevaux, L.: The Hunga Tonga-Hunga Ha'apai Hydration of the Stratosphere, Geophysical Research Letters, 49, https://doi.org/10.1029/2022GL099381, 2022.

Newman, P. A., Nash, E. R., and Rosenfield, J. E.: What Controls the Temperature of the Arctic Stratosphere during the Spring?, Journal of Geophysical Research: Atmospheres, 106, 19 999–20 010, https://doi.org/10.1029/2000JD000061, 2001.

Newman, P. A., Oman, L. D., Douglass, A. R., Fleming, E. L., Frith, S. M., Hurwitz, M. M., Kawa, S. R., Jackman, C. H., Krotkov, N. A., Nash, E. R., Nielsen, J. E., Pawson, S., Stolarski, R. S., and Velders, G. J. M.: What would have happened to the ozone layer if chlorofluorocarbons (CFCs) had not been regulated?, Atmospheric Chemistry and Physics, 9, 2113–2128, https://doi.org/10.5194/acp-9-2113-2009, 2009.

Newman, P. A., Lait, L. R., Kramarova, N. A., Coy, L., Frith, S. M., Oman, L. D., and Dhomse, S. S.: Record High March 2024 Arctic Total Column Ozone, Geophysical Research Letters, 51, e2024GL110 924, https://doi.org/10.1029/2024GL110924, 2024.

NOAA: Antarctic Oscillation (AAO) Index, https://www.cpc.ncep.noaa.gov/products/precip/CWlink/daily_aao_index/teleconnections.shtml, accessed: 20 December 2025, a.

NOAA: Arctic Oscillation (AO) Index, www.cpc.ncep.noaa.gov/products/precip/CWlink/daily_ao_index/teleconnections.shtml, accessed: 20 December 2025, b.

NOAA: NINO3.4 Sea Surface Temperature Anomaly Index Data, https://psl.noaa.gov/data/correlation/nina34.anom.data, accessed: 20 December 2025, c.

Oesterstroem, F. F. and Santee, M. L.: Chapter 6: "Effects of the Hunga eruption on stratospheric ozone and related trace gases" in APARC, 2025: The Hunga Eruption Atmospheric Impacts Report, APARC Report No. 11, WCRP Report No. 10/2025, Forschungszentrum Jülich, https://doi.org/10.34734/FZJ-2025-05242, 2025.

Petropavlovskikh, I., Godin-Beekmann, S., Hubert, D., Damadeo, R., Hassler, B., and Sofieva, V., eds.: SPARC/IO3C/GAW Report on Long-term Ozone Trends and Uncertainties in the Stratosphere, SPARC Report No. 9, GAW Report No. 241, WCRP-17/2018, Deutsches Zentrum für Luft- und Raumfahrt (DLR), https://doi.org/10.17874/F899E57A20B, 2019.

Rahpoe, N., Weber, M., Rozanov, A. V., Weigel, K., Bovensmann, H., Burrows, J. P., Laeng, A., Stiller, G., von Clarmann, T., Kyrölä, E., Sofieva, V. F., Tamminen, J., Walker, K., Degenstein, D., Bourassa, A. E., Hargreaves, R., Bernath, P., Urban, J., and Murtagh, D. P.: Relative Drifts and Biases between Six Ozone Limb Satellite Measurements from the Last Decade, Atmospheric Measurement Techniques, 8, 4369–4381, https://doi.org/10.5194/amt-8-4369-2015, 2015.

Reinsel, G. C., Weatherhead, E., Tiao, G. C., Miller, A. J., Nagatani, R. M., Wuebbles, D. J., and Flynn, L. E.: On Detection of Turnaround and Recovery in Trend for Ozone, Journal of Geophysical Research: Atmospheres, 107, https://doi.org/10.1029/2001JD000500, 2002.

Snow, M., Weber, M., Machol, J., Viereck, R., and Richard, E.: Comparison of Magnesium II core-to-wing ratio observations during solar minimum 23/24, Journal of Space Weather and Space Climate, 4, A04, https://doi.org/https://doi.org/10.1051/swsc/2014001, 2014.

https://doi.org/10.5194/egusphere-2026-2576
Preprint. Discussion started: 11 May 2026

Sofieva, V., Kyrölä, E., Laine, M., Tamminen, J., Degenstein, D., Bourassa, A., Roth, C., Zawada, D., Weber, M., Rozanov, A., Rahpoe, N., Stiller, G., Laeng, A., von Clarmann, T., Walker, K. A., Sheese, P., Hubert, D., Van Roozendael, M., Zehner, C., and Bhartia, P. K.: Merged SAGE II, Ozone_cci and OMPS ozone profile dataset and evaluation of ozone trends in the stratosphere, Atmospheric Chemistry and Physics, 17, 12 533–12 552, https://doi.org/10.5194/acp-17-12533-2017, 2017.

Sofieva, V. F., Szelag, M., Tamminen, J., Arosio, C., Rozanov, A., Weber, M., Degenstein, D., Bourassa, A., Zawada, D., Kiefer, M., et al.: Updated merged SAGE-CCI-OMPS+ dataset for the evaluation of ozone trends in the stratosphere, Atmospheric Measurement Techniques, 16, 1881–1899, https://doi.org/10.5194/amt-16-1881-2023, 2023.

Sofieva, V. F., Rozanov, A., Szelag, M., Burrows, J. P., Retscher, C., Damadeo, R., Degenstein, D., Rieger, L. A., and Bourassa, A.: CREST: a Climate Data Record of Stratospheric Aerosols, Earth System Science Data, 16, 5227–5241, https://doi.org/10.5194/essd-16-5227-2024, 2024.

Sofieva, V. F., Szelag, M. E., Kramarova, N., Damadeo, R., Steinbrecht, W., Petropavlovskikh, I., Vigouroux, C., Maillard Barras, E., Zawada, D., Tourpali, K., Frith, S. M., Wild, J. D., Davis, S. M., Arosio, C., Weber, M., Rozanov, A., Auffarth, B., Froidevaux, L., Fuller, R., Degenstein, D., Dube, K., Effertz, P., Leblanc, T., Ancellet, G., Godin-Beekmann, S., McConville, G., Querel, R., Smale, D., DeBacker, M.-R., Mahieu, E., and Sussmann, R.: Updated Global and Regional Trends of Stratospheric Ozone Profiles, EGUsphere, 2025, 1–25, https://doi.org/10.5194/egusphere-2025-5963, 2025.

Solomon, S.: Stratospheric ozone depletion: A review of concepts and history, Reviews of Geophysics, 37, 275–316, https://doi.org/10.1029/1999RG900008, 1999.

Solomon, S., Kinnison, D. E., Mills, M., Neely, R. R., Schmidt, J., MacKenzie, I. R., Molod, A. M., and Horowitz, L. W.: Emergence of healing in the Antarctic ozone layer, Science, 353, 269–274, https://doi.org/10.1126/science.aae0061, 2016.

Steffen, J., Bernath, P. F., and Boone, C. D.: Trends in Halogen-Containing Molecules Measured by the Atmospheric Chemistry Experiment (ACE) Satellite, Journal of Quantitative Spectroscopy and Radiative Transfer, 238, 106 619, https://doi.org/10.1016/j.jqsrt.2019.106619, 2019.

Steinbrecht, W., Froidevaux, L., Fuller, R., Wang, R., Anderson, J., Roth, C., Bourassa, A., Degenstein, D., Damadeo, R., Zawodny, J., Frith, S., McPeters, R., Bhartia, P., Wild, J., Long, C., Davis, S., Rosenlof, K., Sofieva, V., Walker, K., Hubert, D., Laeng, A., von Clarmann, T., Godin-Beekmann, S., Leblanc, T., Querel, R., Swart, D., Boyd, I., Hocke, K., Kämpfer, N., Maillard Barras, E., Moreira, L., Nedoluha, G., Vigouroux, C., Blumenstock, T., Schneider, M., García, O., Jones, N., Mahieu, E., Smale, D., Kotkamp, M., Robinson, J., Petropavlovskikh, I., Harris, N., Hassler, B., and Hubert, A.: An update on ozone profile trends for the period 2000 to 2016, Atmospheric Chemistry and Physics, 17, 10 675–10 690, https://doi.org/10.5194/acp-17-10675-2017, 2017.

Stolarski, R. S., Douglass, A. R., Steenrod, S., and Pawson, S.: Trends in Stratospheric Ozone: Lessons Learned from a 3D Chemical Transport Model, Journal of the Atmospheric Sciences, 63, 1028–1041, https://doi.org/10.1175/JAS3650.1, 2006.

Stone, K. A., Solomon, S., and Kinnison, D. E.: On the Identification of Ozone Recovery, Geophysical Research Letters, 45, 5158–5165, https://doi.org/10.1029/2018GL077955, 2018.

Szeląg, M. E., Sofieva, V. F., Degenstein, D. A., Roth, C. Z., Froidevaux, L., Davis, S. M., Damadeo, R., Walker, K. A., Hubert, D., Lambert, J.-C., and Zawada, D. J.: Seasonal stratospheric ozone trends over 2000–2018 derived from several merged data sets, Atmospheric Chemistry and Physics, 20, 7035–7047, https://doi.org/10.5194/acp-20-7035-2020, 2020.

Thompson, D. W. J., Solomon, S., Kushner, P. J., England, M. H., Grise, K. M., and Karoly, D. J.: Signatures of the Antarctic ozone hole in Southern Hemisphere surface climate change, Nature Geoscience, 4, 741–749, https://doi.org/10.1038/ngeo1296, 2011.

https://doi.org/10.5194/egusphere-2026-2576
Preprint. Discussion started: 11 May 2026

van der A, R. J., Allaart, M. A. F., and Eskes, H. J.: Extended and refined multi sensor reanalysis of total ozone for the period 1970–2012, https://doi.org/https://doi.org/10.5194/amt-8-3021-2015, 2015.

Velders, G. J. M., Andersen, S. O., Daniel, J. S., Fahey, D. W., and McFarland, M.: The importance of the Montreal Protocol in protecting climate, Proceedings of the National Academy of Sciences, 104, 4814–4819, https://doi.org/10.1073/pnas.0610328104, 2007.

Vömel, H., Evan, S., and Tully, M.: Water Vapor Injection into the Stratosphere by Hunga Tonga-Hunga Ha'apai, Science, 377, 1444–1447, https://doi.org/10.1126/science.abq2299, 2022.

Wang, X., Randel, W., Zhu, Y., Tilmes, S., Starr, J., Yu, W., Garcia, R., Toon, O. B., Park, M., Kinnison, D., Zhang, J., Bourassa, A., Rieger, L., Warnock, T., and Li, J.: Stratospheric Climate Anomalies and Ozone Loss Caused by the Hunga Tonga-Hunga Ha'apai Volcanic Eruption, Journal of Geophysical Research: Atmospheres, 128, e2023JD039 480, https://doi.org/10.1029/2023JD039480, 2023.

Waters, J. W., Froidevaux, L., Harwood, R. S., Jarnot, R. F., Pickett, H. M., Read, W. G., Siegel, P. H., Cofield, R. E., Filipiak, M. J., Flower, D. A., Holden, J. R., Lau, G. K., Livesey, N. J., Manney, G. L., Pumphrey, H. C., Santee, M. L., Wu, D. L., et al.: The Earth Observing System Microwave Limb Sounder (EOS MLS) on the Aura Satellite, IEEE Transactions on Geoscience and Remote Sensing, 44, 1075–1092, https://doi.org/10.1109/TGRS.2006.873771, 2006.

Weber, M., Dikty, S., Burrows, J. P., Garny, H., Dameris, M., Kubin, A., Abalichin, J., and Langematz, U.: The Brewer-Dobson Circulation and Total Ozone from Seasonal to Decadal Time Scales, Atmospheric Chemistry and Physics, 11, 11 221–11 235, https://doi.org/10.5194/acp-11-11221-2011, 2011.

Weber, M., Coldewey-Egbers, M., Fioletov, V. E., Frith, S. M., Wild, J. D., Burrows, J. P., Long, C. S., and Loyola, D.: Total Ozone Trends from 1979 to 2016 Derived from Five Merged Observational Datasets – the Emergence into Ozone Recovery, Atmospheric Chemistry and Physics, 18, 2097–2117, https://doi.org/10.5194/acp-18-2097-2018, 2018.

Weber, M., Coldewey-Egbers, M., Fioletov, V., Frith, S., Wild, J., Burrows, J. P., Long, C., Loyola, D., Degenstein, D., Davis, S. M., Tourpali, K., Steinbrecht, W., and Ball, W. T.: Global total ozone recovery trends attributed to ozone-depleting substance changes derived from five merged ozone datasets, Atmospheric Chemistry and Physics, 22, 6843–6865, https://doi.org/10.5194/acp-22-6843-2022, 2022.

WMO, 2018: Scientific Assessment of Ozone Depletion: 2018, World Meteorological Organization, Global Ozone Research and Monitoring Project – Report No. 58, https://csl.noaa.gov/assessments/ozone/2018/, 2018.

WMO, 2022: Scientific Assessment of Ozone Depletion: 2022, World Meteorological Organization, Global Ozone Research and Monitoring Project – Report No. 59, https://csl.noaa.gov/assessments/ozone/2022/, 2022.

Wolter, K. and Timlin, M. S.: El Niño/Southern Oscillation Behaviour since 1871 as Diagnosed in an Extended Multivariate ENSO Index (MEI.Ext), International Journal of Climatology, 31, 1074–1087, https://doi.org/10.1002/joc.2336, 2011.

Yook, S., Thompson, D. W. J., and Solomon, S.: Climate Impacts and Potential Drivers of the Unprecedented Antarctic Ozone Holes of 2020 and 2021, Geophysical Research Letters, 49, e2022GL098 064, https://doi.org/10.1029/2022GL098064, 2022.

Zhu, Y., Mann, G., Newman, P. A., and Randel, W., eds.: The Hunga Volcanic Eruption Atmospheric Impacts Report, APARC Report 11, Forschungzentrum Jülich, https://doi.org/10.34734/FZJ-2025-05237, 2025.

https://doi.org/10.5194/egusphere-2026-2576
Preprint. Discussion started: 11 May 2026

Appendix

https://doi.org/10.5194/egusphere-2026-2576
Preprint. Discussion started: 11 May 2026

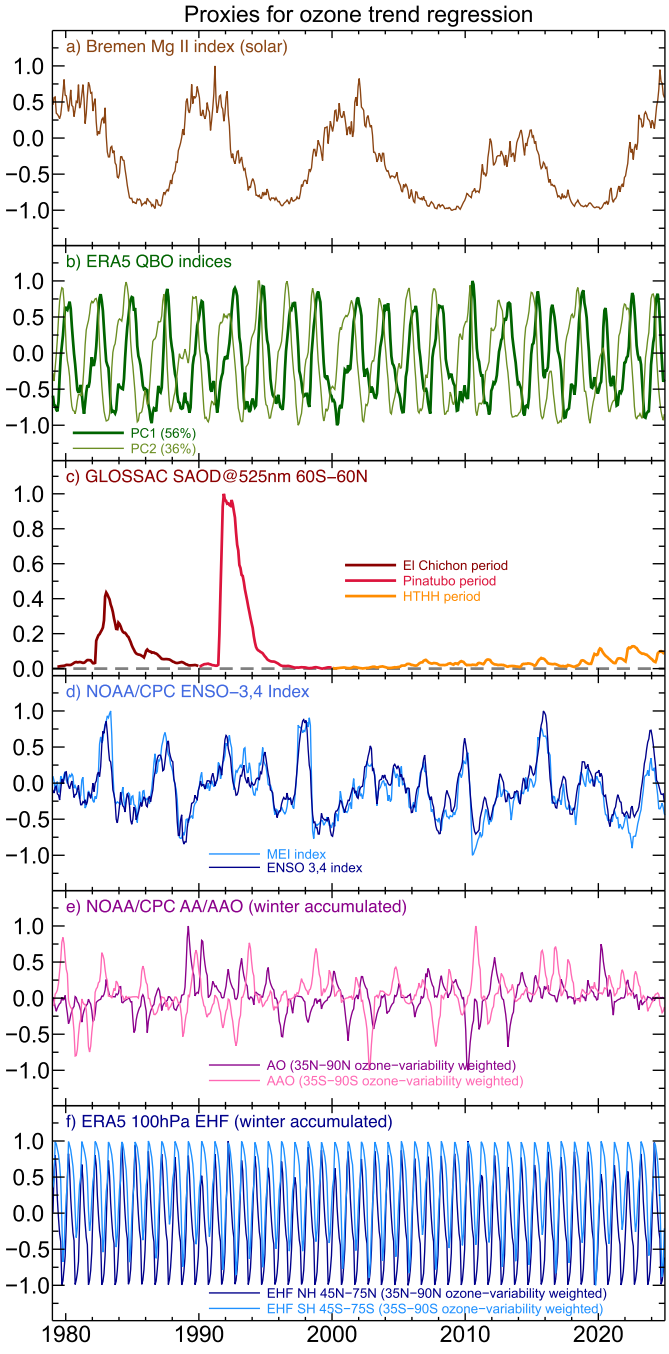

Figure A1. Proxies used in the full regression model. Proxies shown are (a) Solar, (b) QBO1/QBO2, (c) SAOD (with the three periods shown in different colors), (d) ENSO, (e) AO/AAO and (f) EHFN/EHFS. The AO, AAO and EHFn/EHFs are winter/spring accumulated and ozone-variability weighted, as described in Sect. 4.2. Ozone-variability weights are latitude dependent. The SAOD proxies are determined for the latitude bands considered in the MLR.

https://doi.org/10.5194/egusphere-2026-2576
Preprint. Discussion started: 11 May 2026

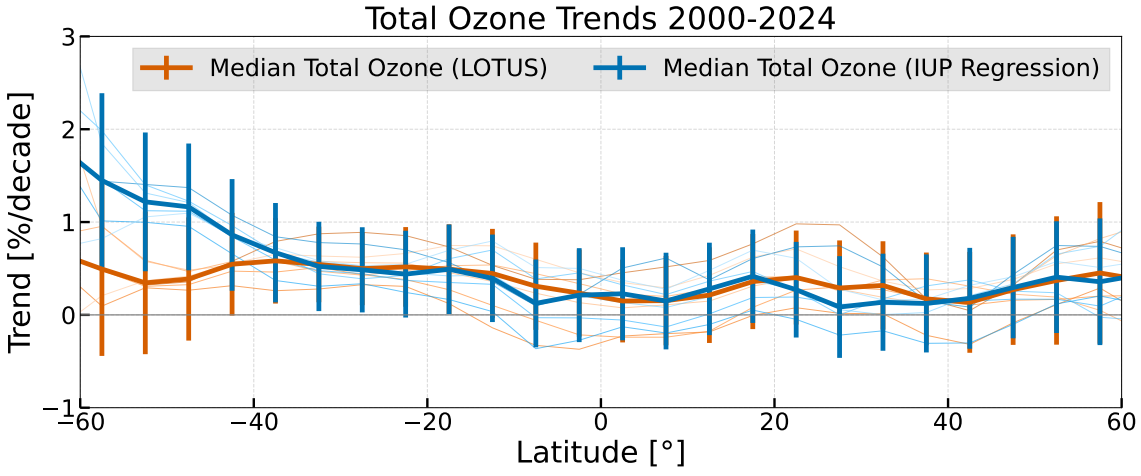

Figure A2. Total ozone trends in %/decade from 2000 to 2024 for the six total ozone datasets WOUDC, SBUV NASA (MOD), SBUV NOAA (COH), GSG, GTO-ECV, and MSR2 (thin lines) and the median and its 2σ uncertainty (thick line and error bars). Shown in blue are the MLR results with additional dynamical and SAOD proxies and in orange the LOTUS model setup. *Same as Fig. 7, but with ozone trend units of %/decade*.

https://doi.org/10.5194/egusphere-2026-2576
Preprint. Discussion started: 11 May 2026

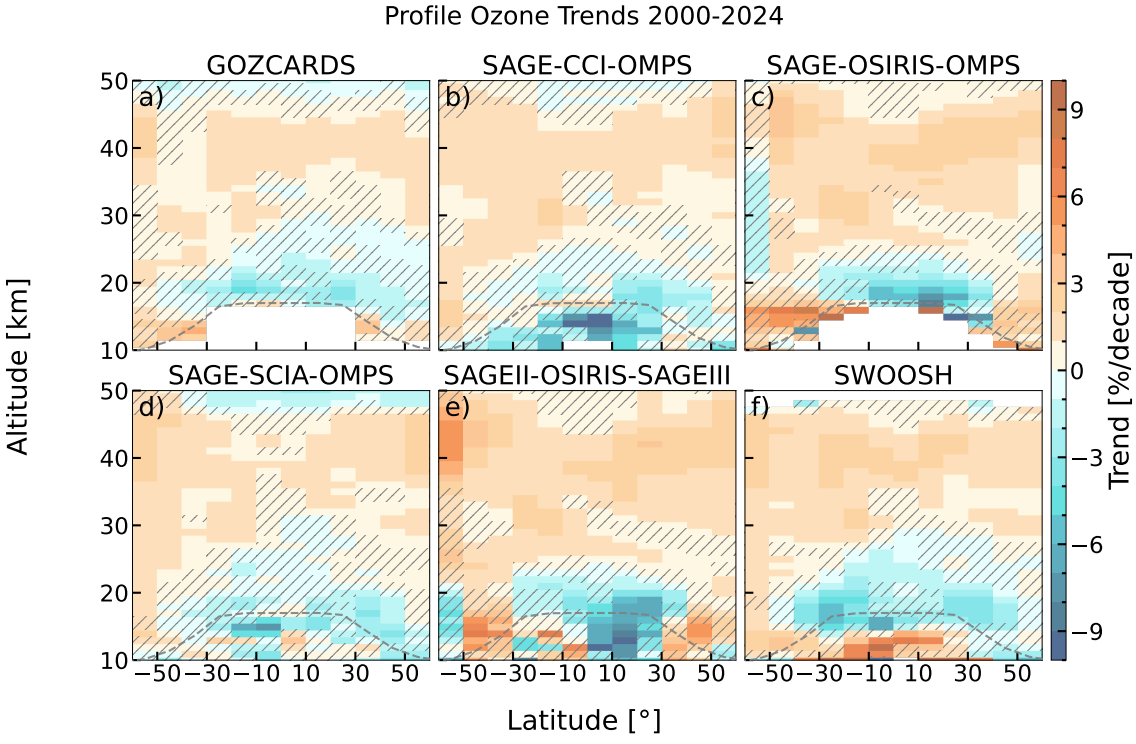

Figure A3. Profile ozone trends in %/decade from 2000 to 2024 for the six profile ozone datasets (a) GOZCARDS , (b) SAGE-CCI-OMPS, (c) SAGE-OSIRIS-OMPS, (d) SAGE-SCIA-OMPS, (e) SAGEII-OSIRIS-SAGEIII, and (f) SWOOSH. Hatches indicate regions of no significance (2σ). *Same as Fig. 9, but in units of %/decade*.

https://doi.org/10.5194/egusphere-2026-2576
Preprint. Discussion started: 11 May 2026

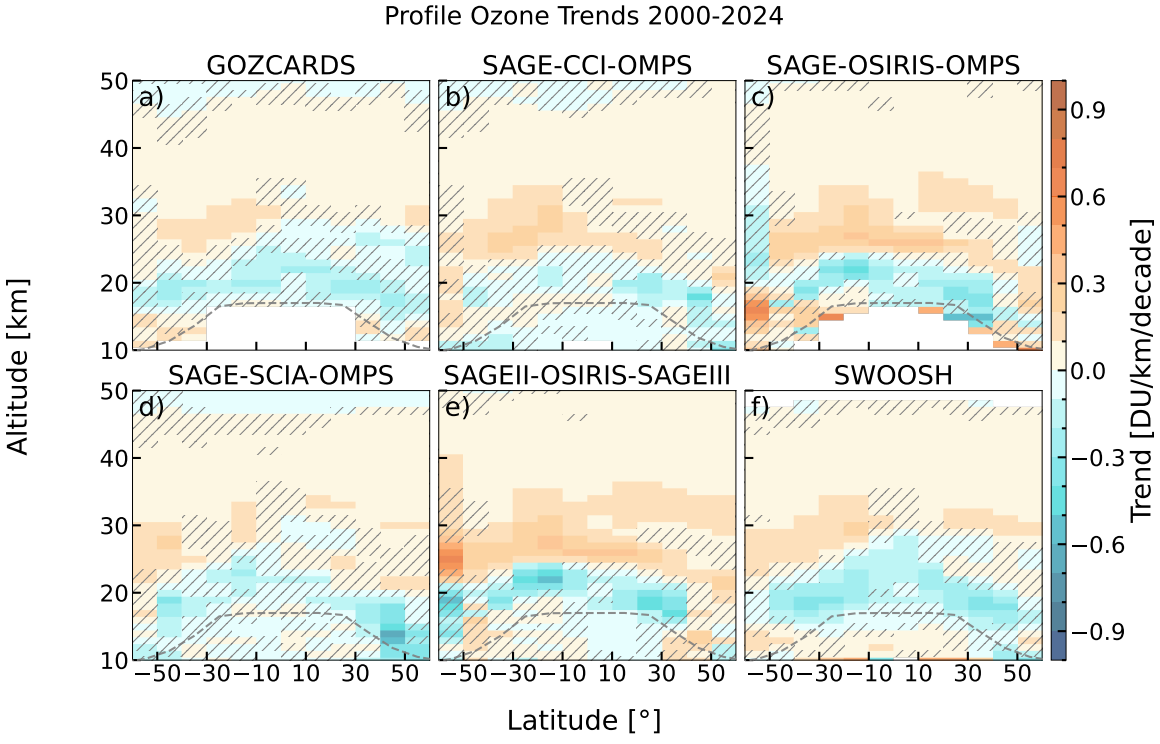

Figure A4. Profile ozone trends (LOTUS model) in DU/km/decade from 2000 to 2024 for the six profile ozone datasets (a) GOZCARDS , (b) SAGE-CCI-OMPS, (c) SAGE-OSIRIS-OMPS, (d) SAGE-SCIA-OMPS, (e) SAGEII-OSIRIS-SAGEIII, and (f) SWOOSH. Hatches indicate regions of no significance (2σ). *Same as Fig. 9, but using the LOTUS setup in the MLR.*

https://doi.org/10.5194/egusphere-2026-2576
Preprint. Discussion started: 11 May 2026

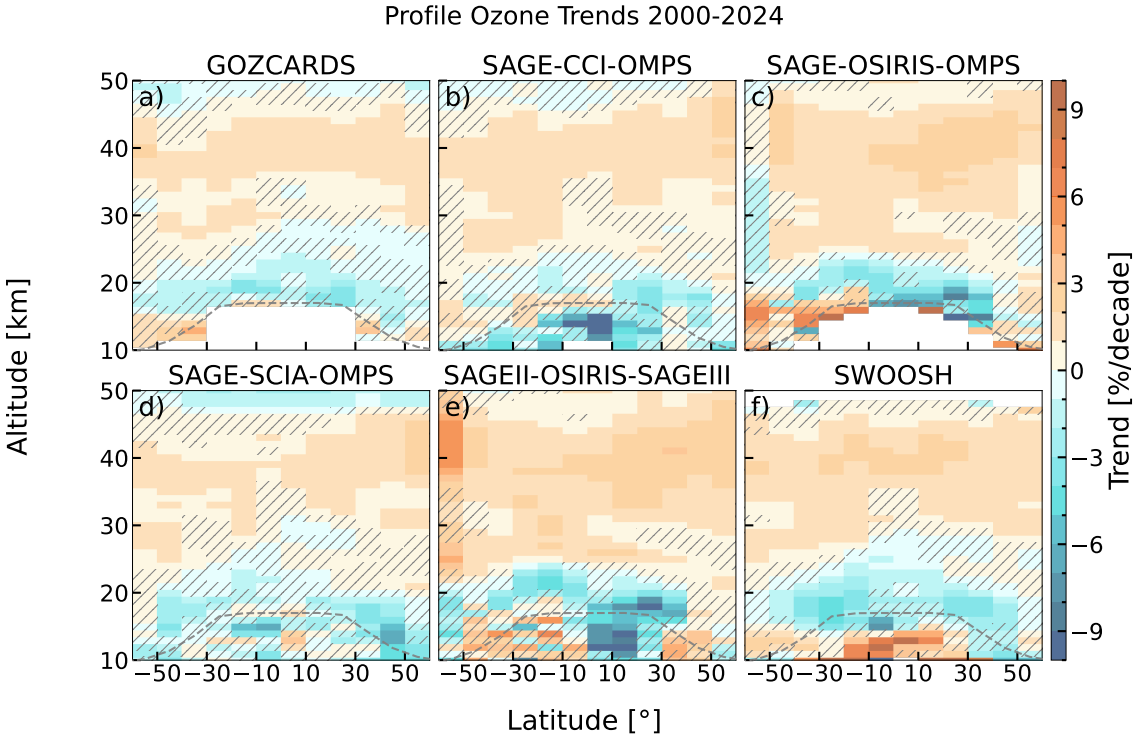

Figure A5. Profile ozone trends in %/decade from 2000 to 2024 using the LOTUS setup for the six profile ozone datasets (a) GOZCARDS , (b) SAGE-CCI-OMPS, (c) SAGE-OSIRIS-OMPS, (d) SAGE-SCIA-OMPS, (e) SAGEII-OSIRIS-SAGEIII, and (f) SWOOSH. Hatches indicate regions of no significance (2σ). *Same as Fig. 9, but using the LOTUS setup in the MLR and trend units of %/decade*.

https://doi.org/10.5194/egusphere-2026-2576
Preprint. Discussion started: 11 May 2026

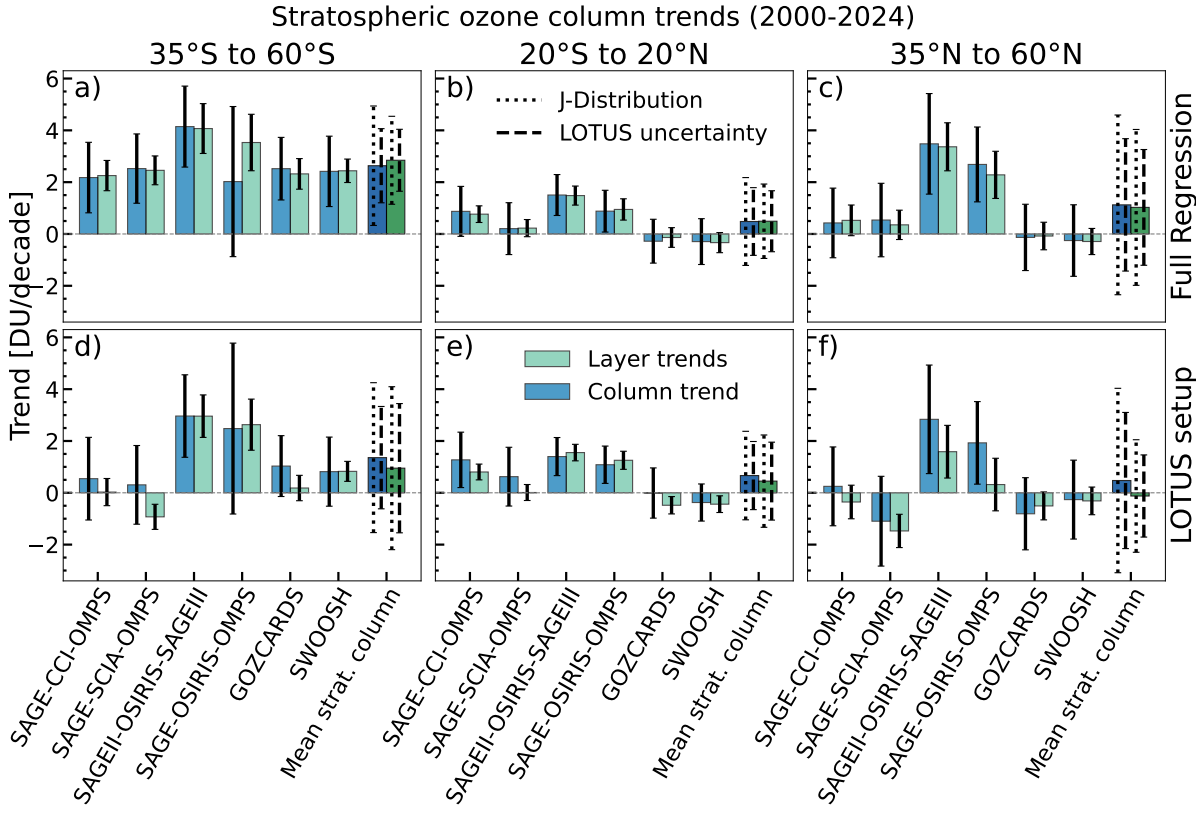

Figure A6. Broad band zonal mean stratospheric ozone column trends from 2000 to 2024. Shown are stratospheric column trends using two approaches: MLR applied to stratospheric columns (dark blue) and stratospheric column trends (light green) determined by integrating ozone layer trends above the thermal tropopause. Upper row panels show the results using the full MLR regression and lower row panels show the regression with the LOTUS setup. Zonal bands are (a,d) 35° S to 60° S, (b,e) 20° S to 20° N, (c,f) 35° N to 60° N. Black error bars indicate the 2σ trend uncertainties. The last two bars in each panel show the mean stratospheric column ozone trends using the two approaches from the six merged datasets with two error bars each calculated using the LOTUS (dashed) and the J-distribution (dotted), respectively.

https://doi.org/10.5194/egusphere-2026-2576
Preprint. Discussion started: 11 May 2026

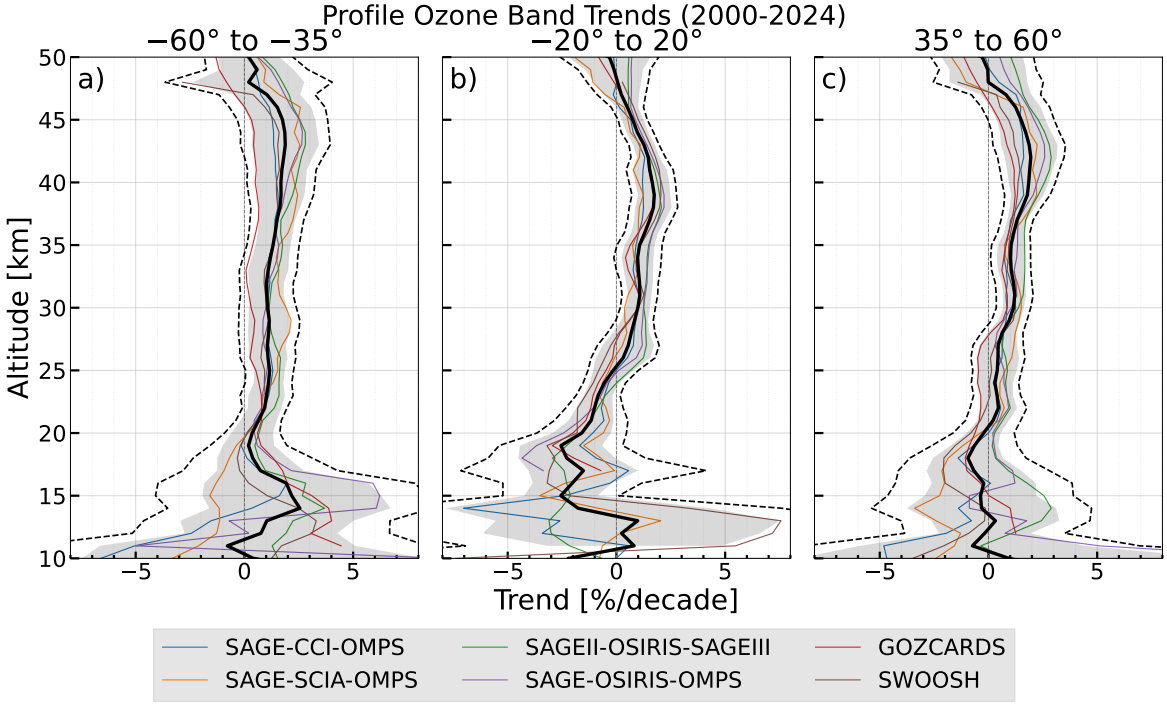

Figure A7. Ozone trends with the IUP Regression Model from 2000 to 2024 in three distinct latitude bands ((a)35°S-60°S, (b) 20°S-20°N, (c) 35°N-60°N) in %/decade for the six merged ozone profile datasets: GOZCARDS, SAGE-CCI-OMPS, SAGE-OSIRIS-OMPS, SAGEII-OSIRIS-SAGEIII, SAGE-SCIA-OMPS, and SWOOSH. Shaded area indicates the 2σ uncertainties, calculated using the LOTUS (Eq. 7) and the dashed line indicates the J-Distribution uncertainty (Eq. 9) of the mean trends (black line). *Same as Fig. 10, but trends in units of %/decade*.

https://doi.org/10.5194/egusphere-2026-2576
Preprint. Discussion started: 11 May 2026

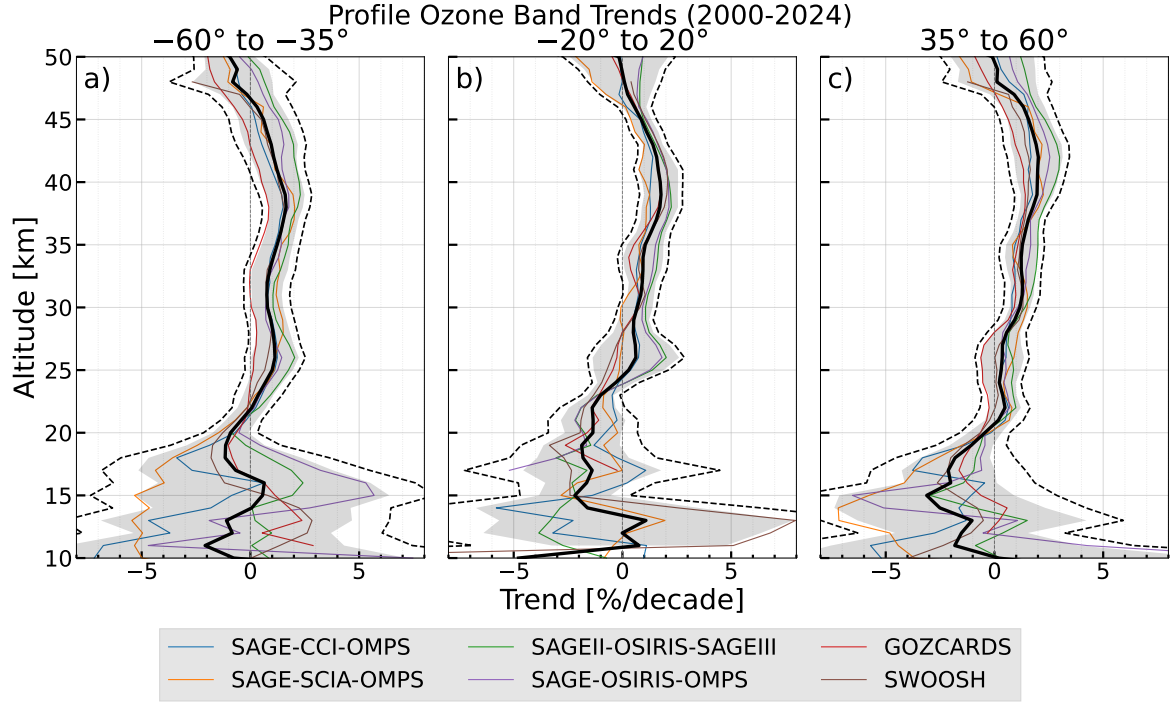

Figure A8. Ozone trends with the LOTUS Model from 2000 to 2024 in three distinct latitude bands ((a)35°S-60°S, (b) 20°S-20°N, (c) 35°N-60°N) in %/decade for the six merged ozone profile datasets: GOZCARDS, SAGE-CCI-OMPS, SAGE-OSIRIS-OMPS, SAGEII-OSIRIS-SAGEIII, SAGE-SCIA-OMPS, and SWOOSH. Shaded area indicates the 2σ uncertainties, calculated using the LOTUS (Eq. 7) and the dashed line indicates the J-Distribution uncertainty (Eq. 9) of the mean trends (black line). *Same as Fig. 10, but using the LOTUS setup in the MLR and trend units of %/decade*.

https://doi.org/10.5194/egusphere-2026-2576
Preprint. Discussion started: 11 May 2026

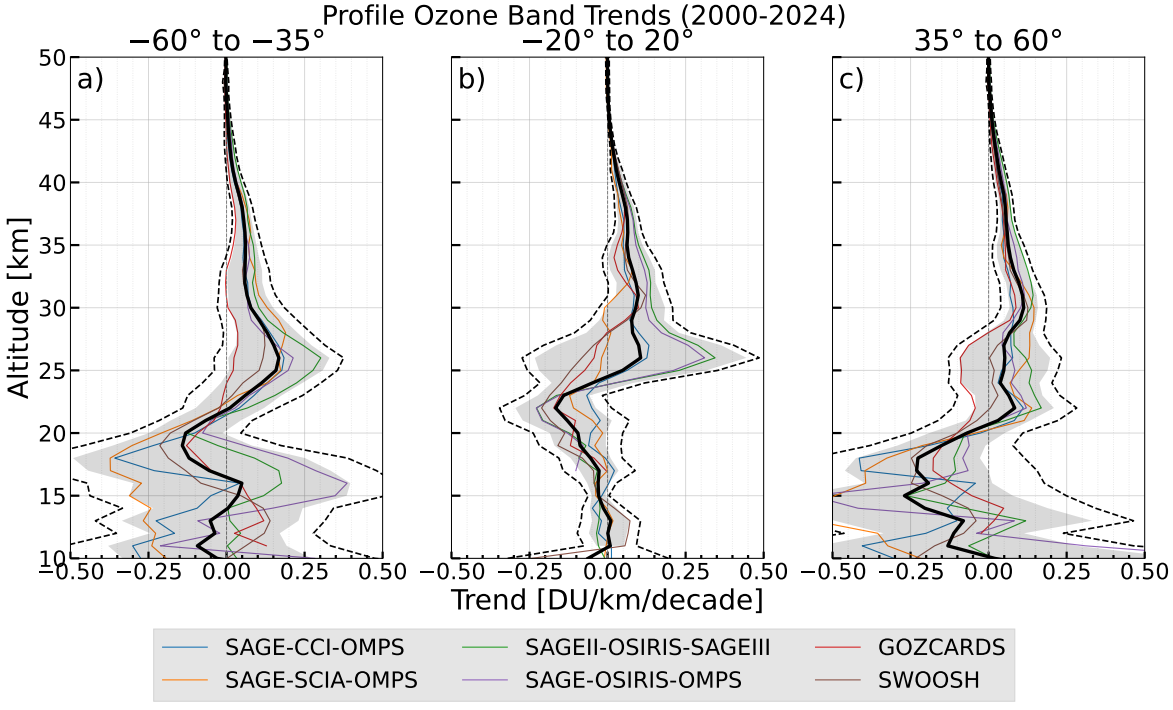

Figure A9. Ozone trends with the LOTUS Model from 2000 to 2024 in three distinct latitude bands ((a)35°S-60°S, (b) 20°S-20°N, (c) 35°N-60°N) in DU/km/decade for the six merged ozone profile datasets: GOZCARDS, SAGE-CCI-OMPS, SAGE-OSIRIS-OMPS, SAGEII-OSIRIS-SAGEIII, SAGE-SCIA-OMPS, and SWOOSH. Shaded area indicates the 2σ uncertainties, calculated using the LOTUS (Eq. 7) and the dashed line indicates the J-Distribution uncertainty (Eq. 9) of the mean trends (black line). *Same as Fig. 10, but using the LOTUS setup in the MLR.*